RECORD
2024/3

THE CHITTERING METAMORPHIC BELT, YILGARN CRATON: STRUCTURAL SETTING, MICROSTRUCTURES AND QUARTZ CRYSTALLOGRAPHIC PREFERRED ORIENTATION

I Zibra and M Peternell

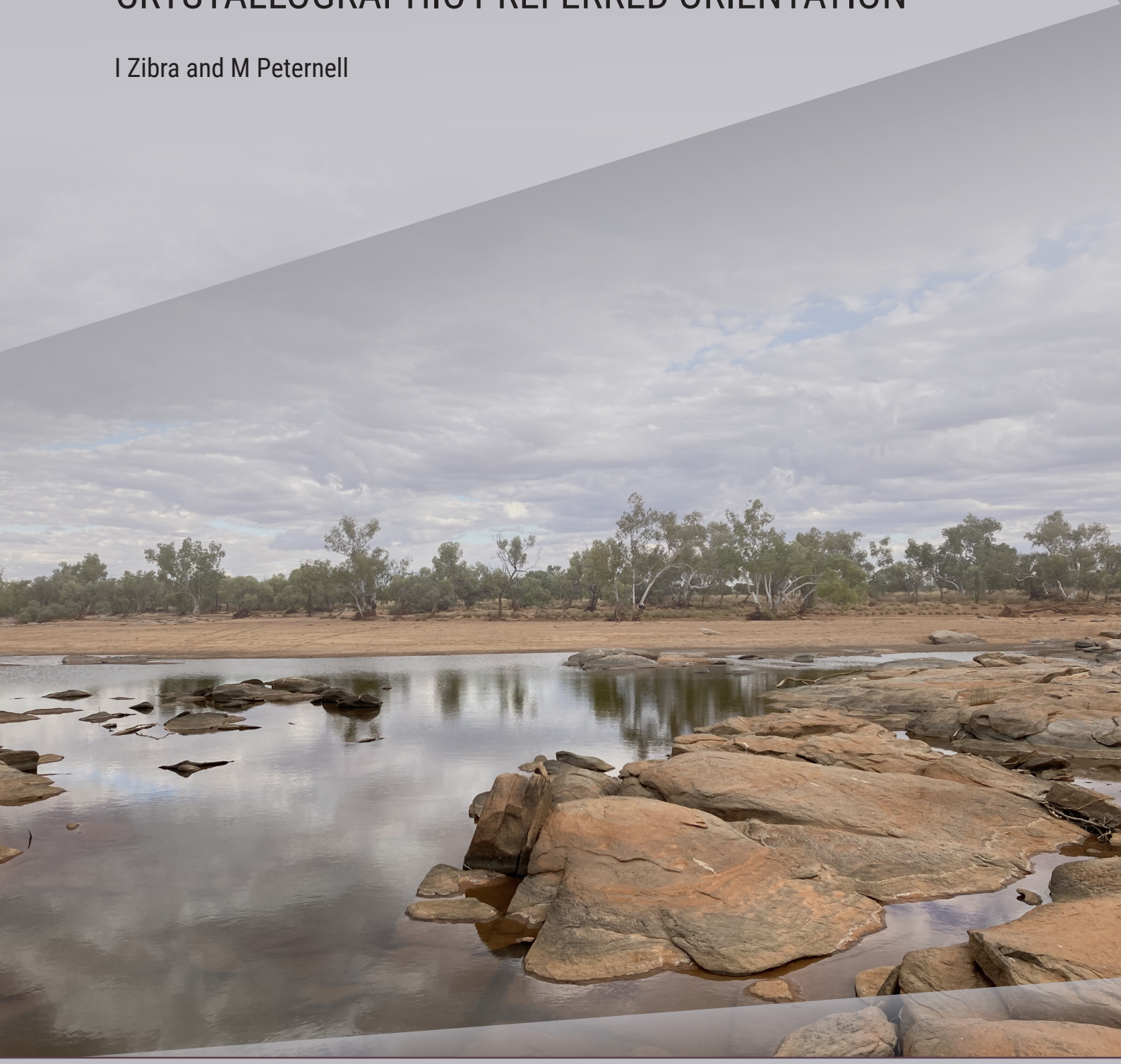

GOVERNMENT OF WESTERN AUSTRALIA
Department of **Energy, Mines, Industry Regulation and Safety**

Geological Survey of Western Australia

Department of **Energy, Mines, Industry Regulation and Safety**

GOVERNMENT OF WESTERN AUSTRALIA

RECORD 2024/3

THE CHITTERING METAMORPHIC BELT, YILGARN CRATON: STRUCTURAL SETTING, MICROSTRUCTURES AND QUARTZ CRYSTALLOGRAPHIC PREFERRED ORIENTATION

I Zibra and M Peternell

PERTH 2024

Geological Survey of Western Australia

REFERENCE
The recommended reference for this publication is:
Zibra, 1 and Peternell, M 2024, The Chittering Metamorphic Belt, Yilgarn Craton: structural setting, microstructures and quartz crystallographic preferred orientation: Geological Survey of Western Australia, Record 2024/3, 31p.

ISBN 978-1-74168-041-6
ISSN 2204-4345

Grid references in this publication refer to the Geocentric Datum of Australia 1994 (GDA94). Locations mentioned in the text are referenced using Map Grid Australia (MGA) coordinates, Zone 50. All locations are quoted to at least the nearest 100 m.

Acknowledgement of Country
We respectfully acknowledge Aboriginal peoples as the Traditional Custodians of this land on which we deliver our services to the communities throughout Western Australia. We acknowledge their enduring connection to the lands, waterways and communities and pay our respects to Elders past and present.

Published 2024 by the Geological Survey of Western Australia
This Record is published in digital format (PDF) and is available online at <www.demirs.wa.gov.au/GSWApublications>.

Further details of geoscience products are available from:
First Floor Counter
Department of Energy, Mines, Industry Regulation and Safety
100 Plain Street
EAST PERTH WESTERN AUSTRALIA 6004
Telephone: +61 8 9222 3459 Email: publications@dmirs.wa.gov.au
www.demirs.wa.gov.au/GSWApublications

Cover image
One of the largest and most distinctive metagranitic units in the Gascoyne Province, the Davy Well Granite emerges from the water of the Yinnetharra Pool along the Gascoyne River. Photo by Angela Riganti

Contents

Abstract 1
Introduction 1
Geological setting 2
Main rock units 2
Map-scale to outcrop-scale structures 10
Ductile structures and fabrics 11
Proterozoic structures and fabrics 11
Archean structures and fabrics 11
Brittle structures and low-temperature shear zones 14
Microstructures and quartz crystallographic preferred orientations 19
Microstructures 19
Proterozoic ductile fabrics 19
Archean ductile fabrics 17
Brittle structures and low-temperature shear zones 21
Quartz crystallographic preferred orientation (CPO) data 21
Discussion and conclusions 28
References 30

Figures

1. Simplified tectonic map of Western Australia, showing the location of the Chittering Metamorphic Belt (CMB) 3
2. Geological map of the CMB 4
3. Outcrop-scale and microscale features of the main layered rock types identified within CMB 6, 8
4. Outcrop-scale and microscale features of the main non-layered rock types identified within the CMB 9, 10
5. Geological map and structural data of the CMB 12, 13
6. Typical outcrop-scale geometry, kinematics and shear sense indicators mapped along the Swan Gorge and the Lady Springs shear zone systems 14, 15
7. Typical outcrop-scale appearance of folds exposed throughout the CMB 16
8. Representative migmatitic structures preserved within the CMB and in the host granites of the Darling Range Batholith 17
9. Equal-area plot of planar and linear structures associated with low-temperature shear zones and faults, exposed along the western margin of the CMB 17
10. Typical outcrop-scale appearance of faults and low-temperature shear zones exposed in leucogranite, along the western margin of the CMB 18
11. Representative example of brittle structures developed on a ductile precursor in leucogranite 19
12. Representative microstructures from the samples collected along Proterozoic shear zones 20
13. Microstructure from samples preserving outcrop-scale evidence of melt-present deformation 21
14. Typical microstructures from low-temperature shear zones 21
15. Quartz CPO data 24
16. Samples showing high-temperature quartz CPO fabrics (group A), with maxima near the x-axis equal area projection plots 25
17. Samples showing a prominent maximum near the y-axis (group B) equal-area projection plots 26
18. Samples showing a transition from maximum near the y-axis to girdle fabric and near-z maxima (group C) equal-area projection plots 27
19. Equal-area projection plots (lower hemisphere, 1% of search area) from samples with maxima scattered throughout the projection plot 27
20. Cartoon illustrating the possible sequence of tectonomagmatic and metamorphic events that led to the assembly and present-day configuration of the CMB 29, 30

Tables

1. Coordinates of outcrops shown in the figures. 5
2. GSWA sample numbers for thin sections shown in this contribution. 5
3. List of GSWA samples analyzed for quartz c-axis CPO 23

The Chittering Metamorphic Belt, Yilgarn Craton: structural setting, microstructures and quartz crystallographic preferred orientation

I Zibra and M Peternell*

Abstract

We present the results from structural mapping and microstructural work focused within the Chittering Metamorphic Belt (CMB), in the Perth hills, bounded to the west by the Mesozoic Darling Fault. This belt represents a portion of the western margin of the Yilgarn Craton of Western Australia, within the northern part of the South West Terrane. The CMB was mapped by the Geological Survey of Western Australia (GSWA) during the 1970s but has not been the target of further systematic geological investigations since. From a lithological viewpoint, the CMB is overwhelmingly dominated by felsic rocks, with mafic rocks being mostly represented by gabbro–dolerite dykes. The main component of the belt is represented by a layered sequence of metasedimentary and metagranitic felsic rocks, which recorded a migmatitic event that predated the emplacement of the late Archean Darling Range Batholith. This association is intruded by two sets of gabbro–dolerite dykes, belonging to the c. 2615 Ma Yandinilling suite and to the c. 1210 Ma Marnda Moorn large igneous province.

Most of the exposed portion of the CMB is dominated by ductile structures. These fabrics are overprinted by northstriking, brittle shear zones and faults, which are restricted to the western portion of the CMB, within 3 km of the Darling Fault, and likely represent small-scale structures associated with this main crustal feature. The regional ductile fabric and the associated main high-strain zones are recorded by the c. 1210 Ma dykes, being therefore of Proterozoic age. We recognise two sets of structures: (i) an oblique-slip (normal–sinistral) shear zone, the Swan Gorge Shear Zone, marks the eastern boundary of the CMB; (ii) a network of anastomosing, strike-slip sinistral shear zones, that are associated with constrictional fabrics, collectively termed the Lady Springs Shear Zone, mainly developed along the western portion of the belt. These two shear zone systems are subparallel to each other being, on average, north-striking, and dipping steeply towards the west (Fig. 5a). However, structures belonging to the two shear zone systems can be differentiated based on the orientation of lineation.

Microstructural data, supported by quartz c-axis crystallographic preferred orientation (CPO) data, show that migmatitic fabrics are locally well-preserved away from the main Proterozoic structures. These shear zones developed under retrograde conditions from amphibolite-facies conditions (in the kyanite stability field) down to greenschistfacies conditions, during the exhumation of the whole belt. We show that the belt-scale layering was already in the current north-striking, steep orientation by the end of the Archean. Such fabric played a fundamental role in controlling the orientation of the Proterozoic ductile fabrics, and of the Mesozoic fabrics associated with the Darling Fault. The CMB preserves the record of tectonomagmatic and metamorphic events that span more than two billion years of Earth's history, making it the ideal target for structural studies focused on structural inheritance.

KEYWORDS: Geological mapping - Structural geology - microstructures - Archean - Proterozoic - Phanerozoic

Introduction

Cratons produce over 90% of the world's gold and platinum, and almost 100% of its diamonds. Furthermore, the properties of cratonic lithospheric roots are becoming increasingly recognized as key factors in the topographical expression of continents (Eaton and Claire Perry, 2013) and the location of many ore deposits (Hoggard et al., 2020). Understanding the role of lithospheric mantle in the stabilization and subsequent preservation of continents requires clarification of the term craton. The original use — kratogen — from the Greek kratos, meaning strong, merely implied a continental terrane displaying long-term stability of hundreds of millions of years. Cratons are distinguished by having anomalously thick lithospheric roots (up to 150 km thick) that are cold, buoyant and rheologically strong (Pearson and Wittig N., 2008). Cratonic mantle owns its physical properties to its high magnesium and low fluid contents, which reflect its chemically depleted nature; in turn, related to the extraction of large volumes, up to 50% (Smithies et al, 2018), of mafic–ultramafic magma to produce greenstone belts, during Archean and Proterozoic times. While these properties explain the longevity and long-term stability of cratons, craton margins are anticipated to be the site of development of large-scale shear belts, which may have experienced repeated episodes of reactivation and reworking, as rigid cratonic blocks drifted on the Earth's surface in a plate tectonics environment, colliding with each other. To test this concept, we have examined in detail the high-strain Chittering Metamorphic Belt (CMB) along the western margin of the Archean Yilgarn Craton.

The CMB is a part of the informally named Balingup subterrane (Wilde et al, 1996), within the South West Terrane of the Yilgarn Craton, and more broadly within the Western

*University of Gothenburg, Universitetsplatsen 1, 405 30 Gothenburg, Sweden

Gneiss Terrane of Gee et al (Gee et al, 1981). The CMB was previously mapped at reconnaissance scale in the 1970s during regional-scale mapping by the Geological Survey of Western Australia (Wilde and Low, 1975). This mapping indicated that the western margin of the Yilgarn Craton was extensively and repeatedly sheared. Ductile shear fabrics have been considered to have formed primarily during the Proterozoic Pinjarra Orogeny (Wilde, 1999; Fitzsimons, 2003; Johnson, 2013), as part of the so-called 'Darling Mobile Belt' (Harris, 1994) or 'Proto-Darling Fault' (Blight et al, 1981); although both Blight et al, and Bretan (1985) suggested that at least part of the shear fabric along this belt is of Archean age. However, neither the number of generations nor the age(s) of the shear fabrics have been well constrained.

Our work comprises a more detailed meso- to microscale examination of the CMB, as a typical segment of the Darling Mobile Belt. We have systematically documented its lithological and structural character; thereby, better constrained (i) the compositions, distributions, and relative ages of the principal rock types; (ii) the geometry, kinematics, finite strain and relative ages of the various shear fabrics, and (iii) the formation temperatures and textural relationships of the metamorphic minerals constituting the various deformation fabrics. To do this, we mapped a broadly rectangular area (Fig. 1) parallel to, and east of the prominent, north-striking Darling Scarp, about 85 km long, north–south; and about 15–20 km wide, east–west. Mapping was done from the Bells Rapids area near Brigadoon in the south (latitude 31°46'S), northwards to just north of the town of Mogumber (latitude 31°02'S), close to the northern margin of the Perth 1:250 000 map sheet (Wilde and Low, 1975). The southern part of the CMB, between the Avon Valley and the southern part of the Chittering Valley, is very well exposed (up to 50% outcrop), but outcrop abundance and quality both progressively decrease northwards, where the landscape has much more subdued relief. This disparity in rock exposure is reflected on the geological map (Fig. 2), in the decreasing density of structural data points and sampling from south to north, and increasing reliance on geophysical data for mapping geology.

Mesoscale observations are supported with petrographic analysis of about 200 thin sections prepared from oriented rock samples collected during mapping. This work includes an evaluation of quartz crystallographic preferred orientations (CPO) from 99 oriented thin sections.

In the following sections, we first describe the regional geological setting of the CMB, then the map-scale distribution, typical meso- to microscale characteristics and mineral assemblage of its main constituent lithological units, then outcrop-scale and microstructural data, including quartz CPO data. We conclude with a discussion of the significance of the results for the geological evolution of the CMB specifically; and more generally for the western margin of the Yilgarn Craton.

Geological setting

The CMB is exposed along the western margin of the Yilgarn Craton (Fig. 1), within the northern portion of the South West Terrane (Quentin de Gromard et al, 2021) The CMB includes a series of metamorphic rocks that are exposed north from Bullsbrook, for about 75 km, to the northern limit of the Perth 1:250 000 map sheet (Wilde and Low, 1975). The average width of the belt is 10 km. The rocks have a northerly regional strike and dip steeply to east or west. The CMB includes a series of high-strain metamorphic rocks that mainly consist of leucocratic gneiss and schist, associated with subordinate mafic gneiss and schist. A north-striking, subvertical foliation and layering are well-developed nearly everywhere throughout the CMB, although we were able to distinguish between domains of relative higher and lower finite strain. Nevertheless, weakly deformed to undeformed rocks are rare, and are mainly represented by the more competent gabbroic lithologies. The sequence is interpreted to have experienced Barrovian-type metamorphism, with development of kyanite, sillimanite, staurolite and garnet in felsic lithologies (Wilde and Low, 1975), although the relative and the absolute timing of this metamorphic event is poorly constrained. Felsic migmatites are described in large portions of the CMB (Wilde and Low, 1975). The Darling Fault marks the western limit of the CMB (Dentith et al, 1993; Middleton et al, 1993), while the southern and eastern flanks of the CMB are intruded by Archean granitic rocks belonging to the 2648–2626 Ma Darling Range Batholith (Nemchin and Pidgeon, 1997). In contrast, the northern portion of the CMB is juxtaposed to greenstone rocks belonging to the Jimperding greenstone belt (Wilde, 2001). As constrained during this mapping project, the contact between the two belts is marked by northwest-striking, low-temperature shear zones, which likely experienced local post-Archean reactivations of the high-temperature Archean, northwest-striking fabrics that characterize the Jimperding greenstone belt.

Field and geophysical data indicate that the CMB and surrounding granitic rocks are intruded by gabbro–dolerite dykes having two main orientations (Fig. 2):

1. northeast-striking, newly-discovered dykes striking N045°–070°, occurring mainly in the southeastern portion of the mapped area. They are correlated on the basis of similar orientation with the c. 2615 Ma Yandinilling dyke swarm intruded into the Jimperding greenstone belt, about 100 km east of Perth (Stark et al, 2018).
2. a dense array of north-striking dykes belonging to the c. 1210 Ma Marnda Moorn large igneous province (Wingate, 2017). A dolerite dyke of the Marnda Moorn large igneous province, sampled in Brigadoon, near the southern end of the area mapped here, returned a magmatic crystallization age of 1214 ±5 Ma (Pidgeon and Cook, 2003).

Main rock units

The CMB is overwhelmingly dominated by felsic rocks. Mafic rocks are subordinate, occurring mostly as discrete Archean and/or Proterozoic gabbro–dolerite dykes, and less commonly as small lenses of mafic gneiss, generally less than a few metres wide. In a few localities, due to poor outcrop conditions, it is unclear whether the exposed mafic gneiss may be sheared dykes, or older rocks interleaved with the felsic gneisses. Notably, the CMB contains none of the rock types considered typical of Archean greenstone belts, such as banded-iron formation (BIF), quartzites and conglomerates, and mafic–ultramafic volcanic and intrusive rocks. Tables 1 and 2 provide coordinates for outcrops shown in the figures, and GSWA sample numbers for micrographs, respectively.

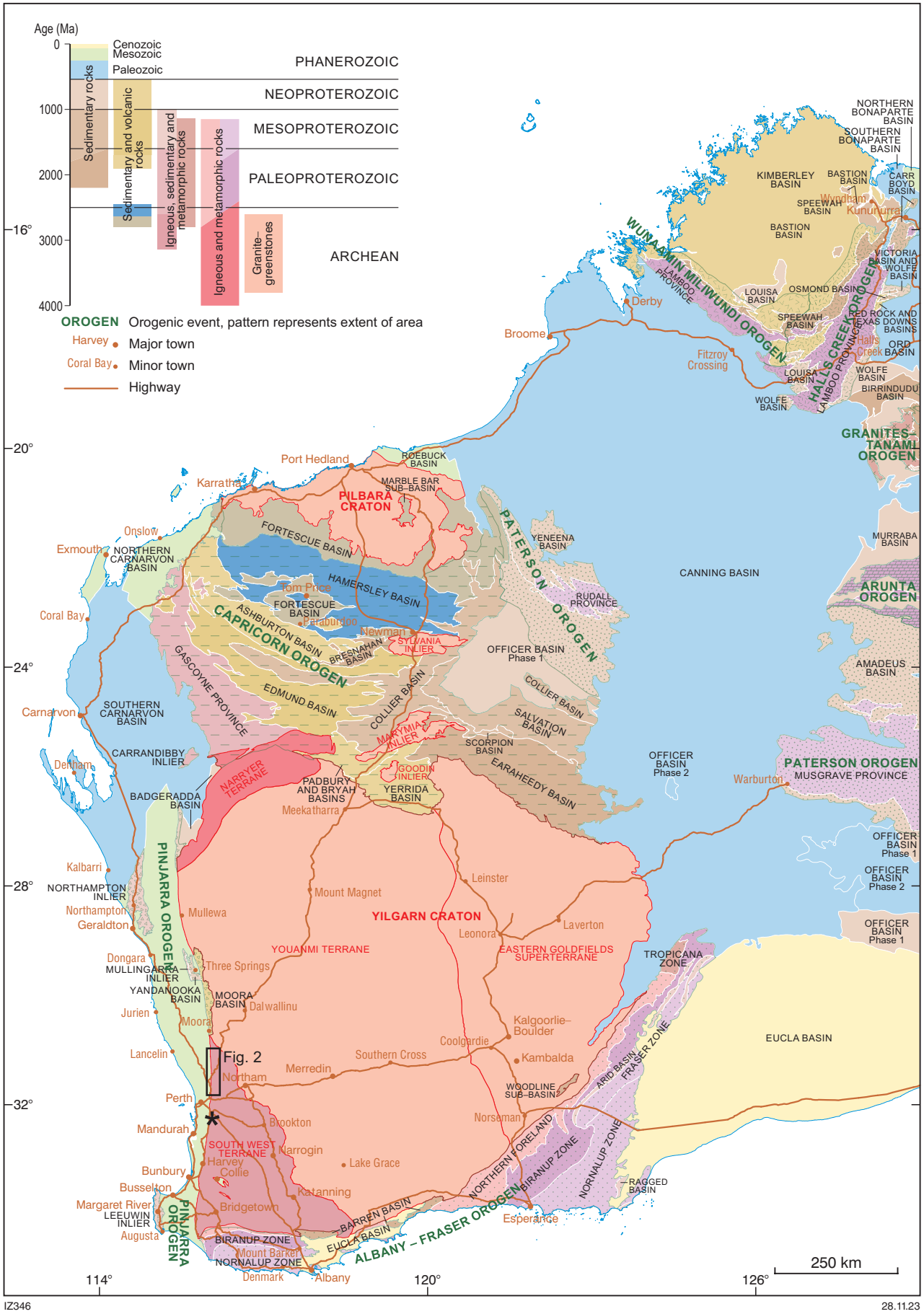

Figure 1. Simplified tectonic map of Western Australia, showing the location of the Chittering Metamorphic Belt (CMB), shown as a black rectangle, along the western margin of the Yilgarn Craton. The asterisk marks the location of the Armadale–Keysbrook area. Modified after Quentin de Gromard et al., 2021.

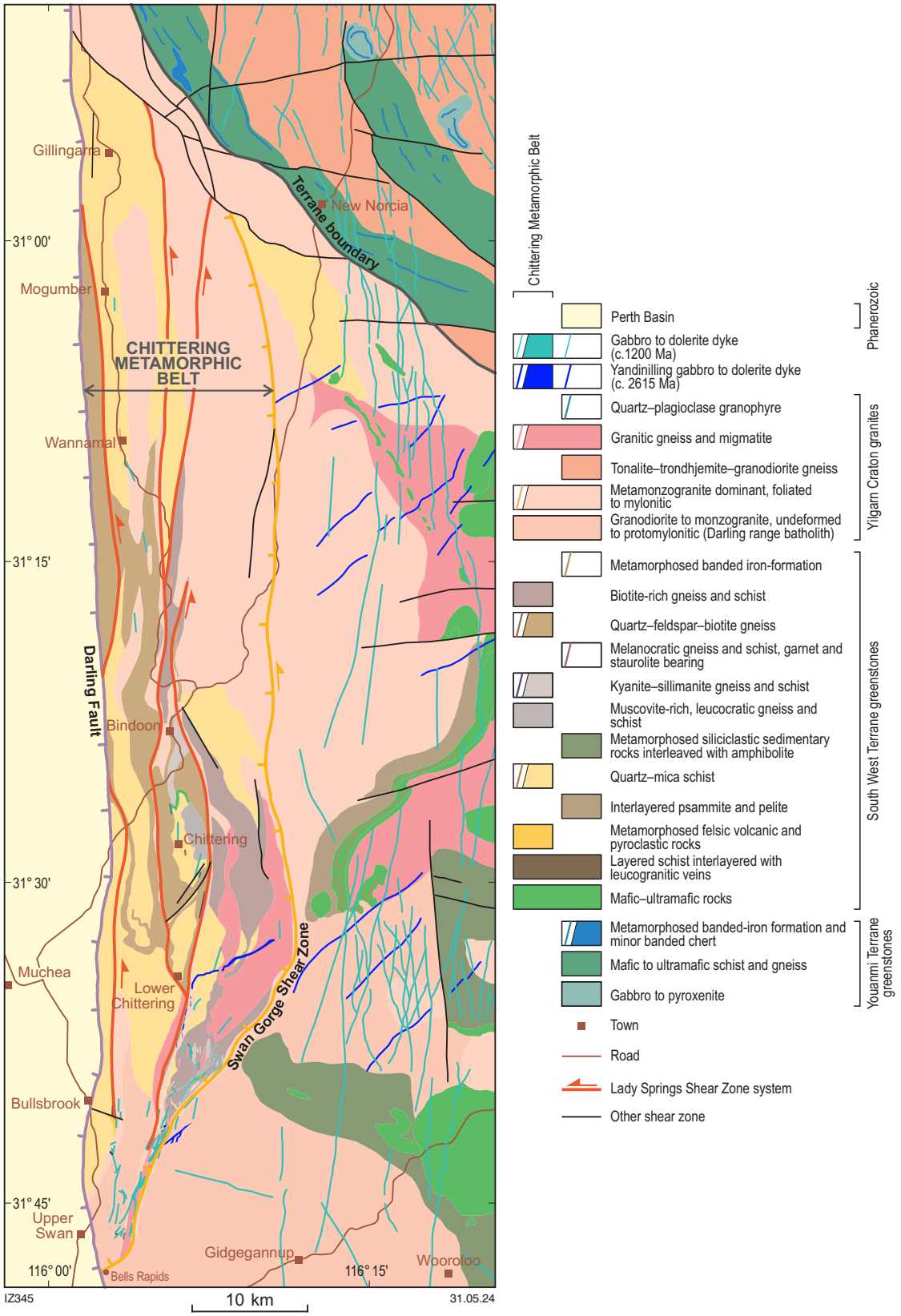

Figure 2. Geological map of the Chittering Metamorphic Belt, developed after Quentin de Gromard et al., 2021.

Felsic gneisses and schists of the CMB can be subdivided into compositionally layered and nonlayered rocks. This is a purely descriptive, field-based classification that helps in identifying the main lithological types within the belt. We combine field data with basic microscope-scale observations, characterize their bulk compositions and the nature of the protoliths.

Table 1. Coordinates of outcrops shown in the figures.

outcrop photo	Latitude	Longitude
3a	-31.601	116.103
3b	-31.601	116.103
3c	-31.724	116.077
3e	-31.640	116.102
3g	-31.629	116.126
3i	-31.263	116.086
3k	-31.643	116.126
3m	-31.707	116.085
4a	-31.173	116.086
4c	-31.435	116.085
4e	-31.601	116.104
4g	-31.263	116.086
4i	-31.391	116.104
4k	-31.628	116.109
6a	-31.743	116.067
6b	-31.775	116.057
6c	-31.724	116.077
6d	-31.774	116.061
6e	-31.777	116.069
6f	-31.601	116.104
6g	-31.365	116.091
6h	-31.602	116.099
6i	-31.575	116.109
6j	-31.573	116.117
7a	-31.773	116.062
7b	-31.697	116.091
7c	-31.708	116.085
7d	-31.629	116.126
7e	-31.306	116.143
7f	-31.396	116.113
7g	-31.263	116.086
7h	-31.390	116.104
8a	-31.629	116.117
8b	-31.696	116.103
8c	-31.640	116.101
8d	-32.108	116.033
10a	-31.741	116.053
10b	-31.741	116.053
10c	-31.711	116.048
10d	-31.711	116.048
10e	-31.741	116.053
10f	-31.742	116.053
10g	-31.741	116.053
10h	-31.741	116.053
11a	-31.744	116.061
11b	-31.744	116.061

Table 2. GSWA sample numbers for thin sections shown in this contribution.

micrograph	GSWA sample
3d	250626
3f	250659
3h	250638
3j	250731
3l	250685
3n	250674
4b	251201
4d	251217
4f	250646
4h	250737
4j	250386
4l	251224
12a	250634
12b	251216
12c	250687
12d	251233
12e	250656
12f	250662
13a	250694
13b	250642
14a	250620
14b	250620

We recognize six compositionally distinct layered rock types:

1. **Granitic migmatite gneiss**. This rock type is well exposed, in a ~50 m wide belt, along the southern portion of the Avon Valley, between Bells Rapids and the Chittering Valley. Smaller slivers are exposed locally throughout the CMB. This gneiss is characterized in outcrop by a prominent compositional layering, with alternating melanocratic (biotite-rich) and leucocratic layers, which are typically 1–30 cm in thickness (Fig. 3a–c). Leucocratic layers are in most places associated with ~1 mm thick, biotite-rich selvedges (Fig. 3a,b). Both layer types range from equigranular to locally porphyritic where there are large Kfeldspar phenocrysts (now porphyroclasts, Fig. 3c,d). The most melanocratic layers contain up to 80% modal biotite (Fig. 3c) and likely represent restitic layers; whereas, the leucocratic layers probably represent sheared leucosomes.
2. **Amphibole-bearing tonalitic migmatite gneiss**. This rock type is volumetrically less abundant than the granitic migmatite gneisses, but is also compositionally layered, though typically more melanocratic due to the higher abundance of amphibole, biotite, titanite and epidote (Fig. 3e,f). Epidote exhibits euhedral shape against biotite, suggesting that it represents a primary magmatic phase of the protolith. Plagioclase is a common porphyroclastic phase, and locally retains its magmatic oscillatory zoning, despite widespread deformation, indicating a primary intrusive protolith for this rock unit.

Figure 3. Outcrop-scale and microscale features of the main layered rock types identified within the CMB: a) layered granitic migmatite gneiss, showing its typical centimetre-to-decimetre-scale compositional layering, with alternating melanocratic (biotite-rich) and leucogranitic layers; b) close-up view from the same outcrop shown in a), highlighting the competency contrast between the stronger leucocratic layers (which are boudinaged) and the weaker, biotite-rich layers; c) close-up view of a melanocratic layer, which contains up to 90% biotite, probably representing a restitic layer resulting from migmatization; d) typical microstructure of layered migmatite gneiss shown in a), with plagioclase (Pl) and K-feldspar (Kfs) porphyroclasts wrapped by quartz ribbons (Qtz). Crossed polars in all micrographs presented here, unless indicated; e) typical appearance of the amphibole-bearing tonalitic migmatite gneiss, with layering defining refolded folds; f) typical microstructure of layered migmatite gneiss shown in e), with hornblende (Hbl) and titanite (Ttn) aggregates surrounded by plagioclase (Pl) and quartz porphyroclasts.

3. **Two-mica, tonalitic migmatite gneiss**. This rock type also displays alternating melanocratic and leucocratic layers (Fig. 3g), with the latter likely representing sheared leucosomes. Constituent minerals include plagioclase, quartz and variable proportions (10–50%) of muscovite and biotite (Fig. 3h), and there is no amphibole. Plagioclase porphyroclasts locally retain their magmatic oscillatory zoning, indicating an intrusive igneous protolith.
4. **Garnet–biotite migmatitic schist**. This rock type constitutes a single unit about 50 m thick, cropping out in the northwestern portion of the CMB, about 10 km south from the town of Wannamal, and 3 km east of the Darling Fault. Compositional layering is defined by alternating melanocratic and leucocratic layers (Fig. 3i), though each type has a bulk granitic assemblage, with melanocratic layers markedly enriched in biotite, and leucocratic ones (former leucosomes?) containing garnet porphyroblasts 5–10 mm in size (Fig. 3i,j).
5. **Two-mica quartz schist**. This rock type is exposed in 1–50 m wide layers throughout the CMB, and shows a prominent compositional layering marked by leucocratic quartzite layers and melanocratic quartz schist layers (Fig. 3k,l). The latter contain abundant muscovite and biotite, and locally subordinate kyanite and/or sillimanite. The high quartz content (50–100%) and lack of feldspar suggest that the protolith to this metamorphosed and sheared rock type was probably a compositionally mature sedimentary rock.
6. **Microgranite schist**. This rock type is exposed along the Avon Valley, between Bells Rapids and Syd's Rapids. It shows a prominent compositional layering marked by alternating bluish microgranitic layers and white-to-cream coarser-grained layers showing granitic mineralogy (Fig. 3m). Thin section observations reveal that the rock has a quartzofeldspathic assemblage which has recorded important grain-size reduction (Fig. 3n) as a consequence of intense shearing.

The compositional layering in all these units is likely the end product of solid-state shearing on pre-existing migmatitic fabrics, as discussed in more detail in the section "Microstructures and quartz crystallographic preferred orientations".

We also recognize six non-layered rock types:

1. **Amphibole-bearing porphyritic granitic gneiss**. This rock type is mainly exposed in the central and western portion of the CMB, and is a high-strain, relatively melanocratic granitic gneiss (Fig. 4a). Thin sections reveal the presence of green-to-blue amphibole, with biotite, titanite and epidote aggregates, wrapping around K-feldspar porphyroclasts (Fig. 4b).
2. **Magnetite-bearing microgranitic gneiss**. This rock type is mainly exposed in the central and western part of the CMB, where it chiefly occurs as high-strain, grey–bluish, finegrained rock (average grain size ≤1 mm), with distinctive magnetite grains of up to 1 cm (Fig. 4c). In thin section, this unit reveals a bulk granitic mineralogy, relatively uniform grain size, and foliation highlighted by biotite flakes (Fig. 4d). Wilde and Low (1975) mapped this unit as a granofels due to its common lack of foliation, but this grey microgneiss is, in fact, mainly exposed along constrictional, sinistral shear zones and, therefore, mainly occurs as L>S tectonites to pure L tectonites, accounting for the general lack of planar fabrics (see the section "Microstructures and quartz crystallographic preferred orientations" for a more detailed description).
3. **Two-mica, equigranular granitic gneiss**. This rock type is widely exposed throughout the CMB, as a fine-grained leucogranite with submillimetric feldspar porphyroclasts (Fig. 4e). Thin section reveals a bulk granitic assemblage, with plagioclase and K-feldspar porphyroclasts wrapped by quartz ribbons, and biotite and muscovite flakes (Fig. 4f).
4. **Kyanite–staurolite–biotite schist**. This rock type is exposed in the northwestern CMB, about 10 km south of the town of Wannamal and about 3 km east of the Darling Fault. It comprises a layer about 50 m thick, in contact to the east with the garnet–biotite migmatitic schist, and consists of a biotite-rich, schistose matrix hosting sporadic kyanite and subordinate staurolite porphyroblasts up to 5 cm (Fig. 4g). Thin section shows that the kyanite and staurolite are poikiloblastic, containing inclusions of recrystallized and foliated matrix that is aligned obliquely to the quartz–mica matrix that wraps around the porphyroblasts (Fig. 4h). The abundance of quartz and the lack of feldspar suggest that the protolith was probably a compositionally mature sedimentary rock.
5. **Two-mica, kyanite–sillimanite quartz schist**. This rock type occurs in exposures that are scattered throughout the CMB. The freshest and most prominent outcrops occur on Bindoon Hill, where the rock is a strongly foliated mica schist containing colourless to whitish elongate kyanite porphyroblasts that vary from strongly aligned with mica to define the foliation and lineation, to randomly oriented (Fig. 4i). Thin section shows a muscovite–biotite–quartz matrix wrapping around poikiloblastic kyanite, that is locally replaced by sillimanite (Fig. 4j). Quartz content is up to 75% modal, and there is no detectable feldspar, suggesting a sedimentary and compositionally mature protolith.
6. **Garnet–staurolite–biotite gneiss**. This rock type has been observed in just a single, small (10 m wide), lensoid outcrop within the two-mica tonalitic gneiss, in the southern Chittering Valley. It consists of elongate melanocratic lenses containing garnet, staurolite and biotite aggregates, surrounded by coarse-grained quartz ribbons (Fig. 4k,l).

None of the non-layered rock types show migmatitic fabrics. Some were probably originally intrusive, as indicated by the occurrence of plagioclase with relict magmatic oscillatory zoning and bulk tonalitic-to-granitic mineral assemblages. In contrast, quartz schists containing up to 80% modal quartz, with subsidiary mica, sporadic aluminosilicates, and typically no feldspar, probably had a sedimentary protolith.

Well-exposed granitic rocks of the Darling Range Batholith intrude the rocks of the CMB in its southern part. These granites are mostly medium- to fine-grained equigranular, two-mica leucogranites that are weakly foliated to completely undeformed, but they commonly contain rafts of migmatite gneiss and schist that become more common close to intrusive contacts with the CMB, and can themselves transition to strongly foliated to mylonitic along their contacts with CMB schists and gneisses (a well-exposed example of this transition is in the Bells Rapids' area).

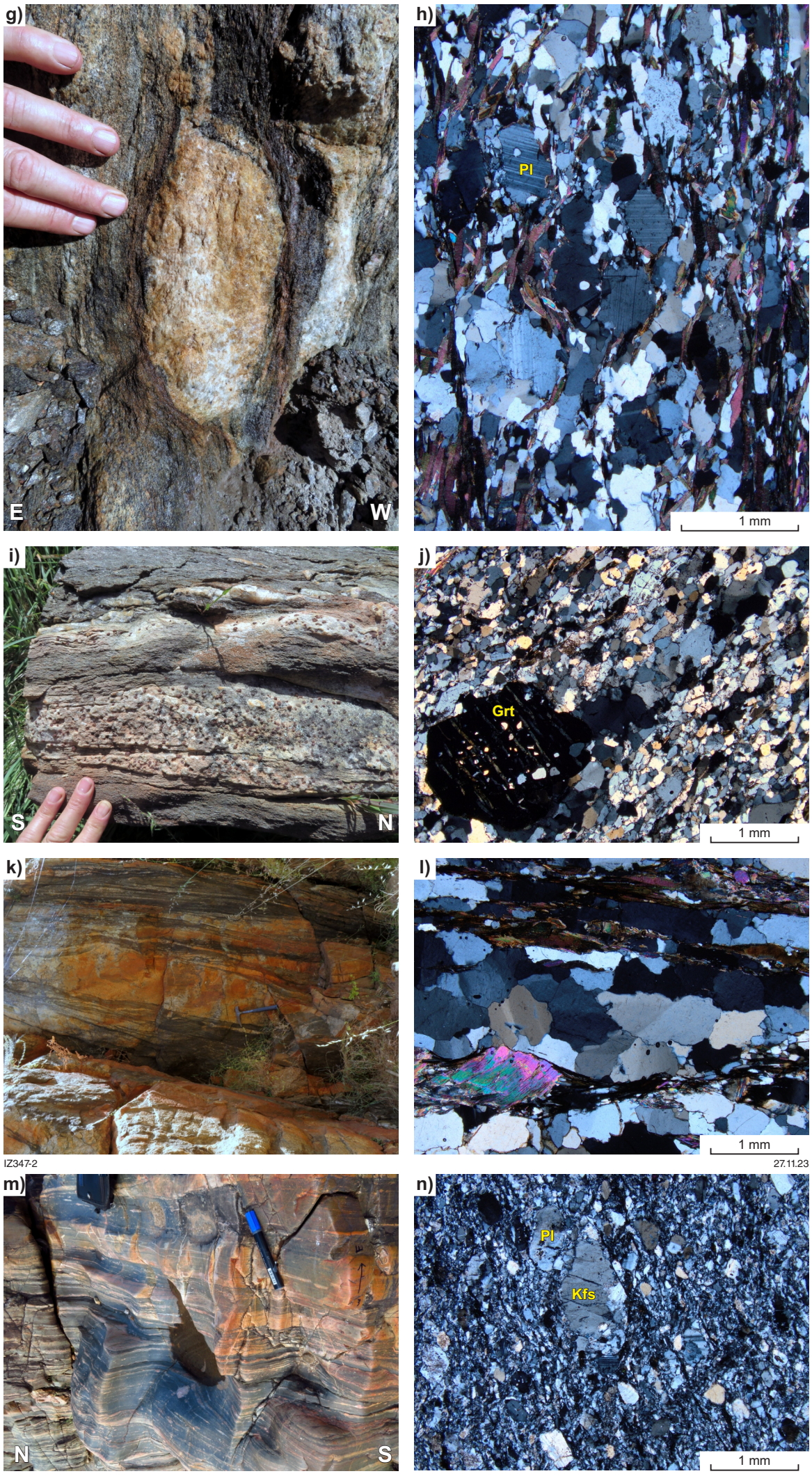

Figure 3. (continued) g) two-mica tonalitic migmatite gneiss with boudinaged leucogranitic layers (former leucosomes?). Melanocratic layers show high mica contents; h) typical microstructure of the two-mica tonalitic migmatite gneiss shown in g), showing plagioclase (Pl) and quartz porphyroclasts wrapped by muscovite and biotite flakes; i) prominent layering of garnet–biotite migmatitic schist, with biotite-rich layers alternating with garnet-bearing leucogranitic layers; j) typical microstructure of garnet–biotite migmatitic schist, from the outcrop shown in i). Garnet porphyroblasts (Grt) are wrapped by the quartzofeldspathic matrix; k) prominent compositional layering in two-mica quartz schist, with interleaved quartzitic leucocratic layers and quartz schist, mica-rich melanocratic layers; l) typical microstructure of a melanocratic layer from the two-mica quartz schist shown in k), with quartz ribbons alternating with layers composed by mica aggregates; m) outcrop-scale appearance of microgranite schist, exposed along the Avon Valley. Bluish microgranitic layers are interleaved with white–cream, coarser-grained granitic layers; n) typical microstructure of a bluish layer of the microgranitic schist shown in m), with plagioclase (Pl) and K-feldspar (Kfs) porphyroclasts wrapped by the fine-grained recrystallized granitic matrix.

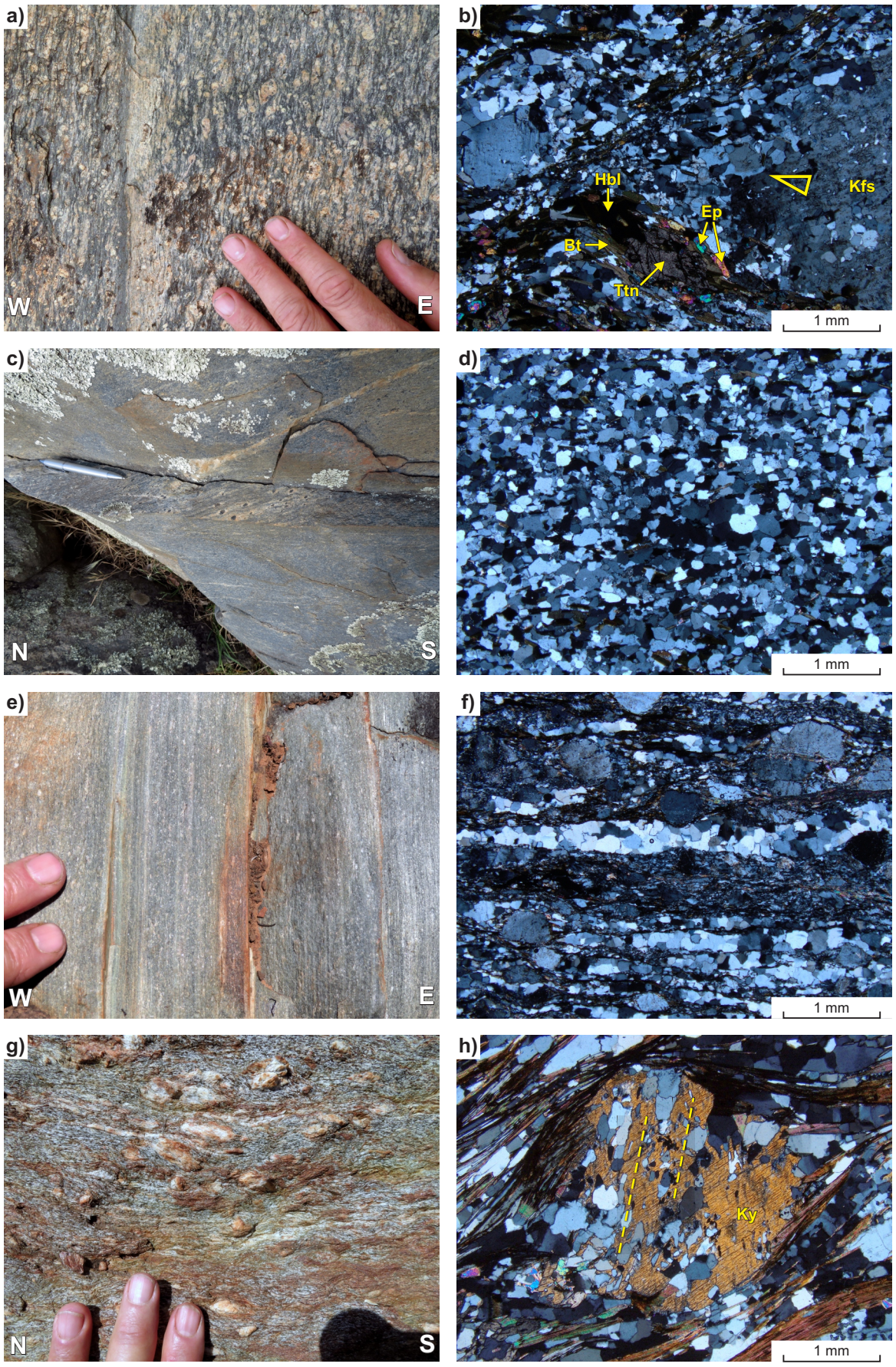

Figure 4. Outcrop-scale and microscale features of the main non-layered rock types identified within the CMB: a) typical outcrop-scale appearance of amphibole-bearing porphyritic granitic gneiss, here intruded by an aplite vein. Rounded K-feldspar porphyroclasts represent former phenocrysts of magmatic origin; b) typical microstructure of porphyritic granitic gneiss, with amphibole (Hbl), titanite (Ttn), biotite (Bt) and epidote (Ep) aggregates wrapping around Kfeldspar porphyroclasts. The larger hollow arrowhead points to coarsegrained recrystallized K-feldspar; c) outcrop-scale appearance of magnetite-bearing microgranitic gneiss; d) typical microstructure of magnetite-bearing microgranitic gneiss, with relatively homogeneous grain size, and with foliation highlighted by biotite flakes; e) outcropscale appearance of two-mica equigranular granitic gneiss, with lensoid whitish layers represented by submillimetric feldspar porphyroclasts, wrapped by recrystallized feldspar tails; f) microstructure from the two-mica equigranular granitic gneiss shown in e), with feldspar porphyroclasts wrapped by quartz ribbons and biotite–muscovite aggregates; g) kyanite–staurolite–biotite schist, showing quartz-mica matrix and scattered kyanite (white) and staurolite (brown-weathered) porphyroblasts; h) microstructure from the outcrop shown in g), showing kyanite porphyroblasts wrapped by quartz-mica matrix. Broken lines mark the trace of the internal foliation in the porphyroblast.

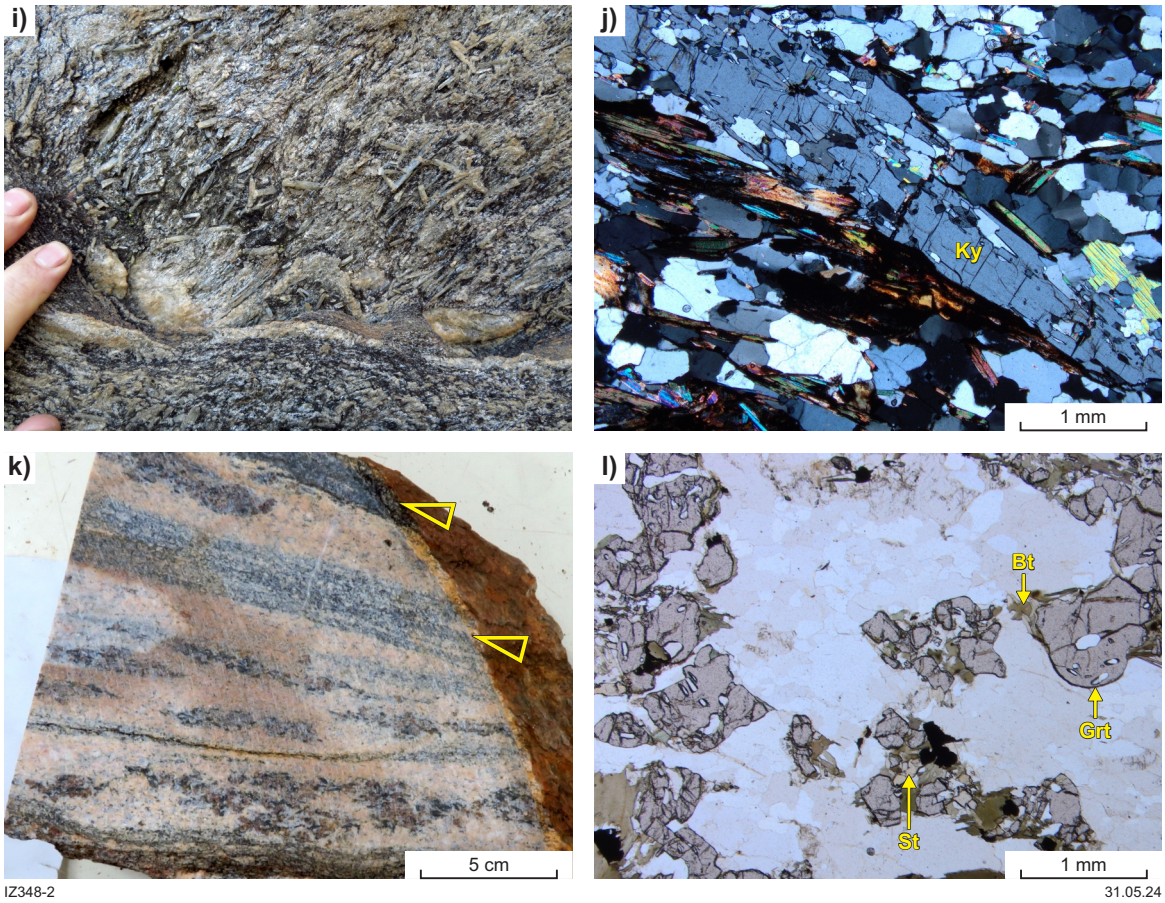

Figure 4. (continued) i) outcrop features of two-mica, kyanite–sillimanite quartz schist from Bindoon Hill, here shown in a foliation-parallel view. Most elongate kyanite porphyroblasts plunge at about 45° to the left, defining the mineral lineation; whereas, other grains have a more dispersed orientation of their long axis; j) microstructure from the outcrop shown in i), elongate kyanite porphyroblasts parallel to biotite and muscovite aggregates, and elongate quartz ribbons; k) hand sample of garnet–staurolite–biotite gneiss. Hollow arrowheads point to layers of two-mica tonalitic gneiss; l) microstructure from the sample shown in k) showing lensoid aggregates of garnet (Grt), staurolite (St) and biotite (Bt) isolated within coarse-grained quartz ribbons. Plane polarized light.

Map-scale to outcrop-scale structures

Geological mapping included systematic collection of planar and linear orientation data (foliation, fold axial plane, mineral and stretching lineation, and fold axis), together with the collection of oriented samples for microstructural work. Most outcrops offered well-developed SL tectonites, in which both foliation and mineral or stretching lineation are well developed. In these cases, we performed shear sense determinations on natural exposures perpendicular to the foliation and parallel to the lineation; that is, parallel to the XZ section of the finite strain ellipsoid (FSE), by using standard kinematic indicators such as σ- and δ-type mantled porphyroclast systems; S–C and C' subfabrics; monoclinic symmetry of folds and boudins; and oblique foliation (Passchier and Trouw, 2005). In those outcrops in which the lineation was not exposed, we performed shear sense determination after cutting an oriented sample (in the laboratory), along the XY and then XZ section of the FSE.

We differentiate here between ductile and brittle structures. This classical subdivision is not devoid of issues and ambiguity, given that these definitions are scale-dependent: a macroscopically ductile shear zone can, for example, be dominated by brittle processes at the grain scale. Furthermore, depending on metamorphic conditions, fluid availability and strain rate, brittle deformation in the stronger phases (e.g. feldspar, amphibole or pyroxene) can coexist with ductile deformation of weaker phases, such as quartz and mica (Passchier and Trouw, 2005). Therefore, in this contribution, the terms 'ductile fabric' and 'ductile shear zone' are used for structures exhibiting dominantly ductile behaviour *at the scale of the outcrop*, regardless of the dominant grain-scale deformation mechanism. The terms 'brittle fabric' and 'brittle shear zone' indicate structures in which brittle deformation manifestly dominates at outcrop scale. Brittle shear zones can also be described as 'a discontinuity with wall-parallel displacement dominated by brittle deformation mechanisms' (Fossen, 2016). The term 'discontinuity' highlights here the observation that faults typically cut off rock layers, making them discontinuous.

The bulk of the outcropping CMB is dominated by ductile structures. These fabrics are overprinted by north-striking, brittle shear zones and faults that are mostly in the western portion of the CMB and are particularly well exposed in granitic rocks of the Darling Range Batholith, along the Darling Scarp between Bullsbrook and Bells Rapids.

Ductile structures and fabrics

Proterozoic structures and fabrics

There are two major Proterozoic ductile shear zone systems in the CMB (Fig. 2) These are subparallel to each other; on average, being north-striking and dipping steeply towards the west (Fig. 5a). However, structures belonging to the two shear zone systems can be differentiated on the basis of lineation orientation and the shape of the FSE. The Swan Gorge Shear Zone (SGSZ) is an oblique-slip (normal–sinistral) shear zone (Fig. 5) that is best developed along the eastern margin of the CMB, juxtaposing this high-strain belt against the lower strain Jimperding greenstone belt, which itself retains Archean magmatic and tectonic fabrics with minimal post-Archean overprint (Wilde and Low, 1975). The SGSZ is well exposed between Bells Rapids and Chittering Valley, and its southern segment largely corresponds to the 'Swan Gorge shear zone' of Wilde and Low (1975); hence, this name is retained. Rocks exposed along the SGSZ are SL tectonites (i.e. foliation and lineation are developed with comparable intensity), with steeply south-plunging mineral and stretching lineations (Fig. 5b, and Fig. 6a,b). S–C fabric and C' shear bands consistently indicate obliqueslip (sinistral, west-side-down) kinematics steeply south-dipping exposures (Fig. 6c,d). Ductile structures with similar geometry and kinematics (albeit generally lower finite strain) to the SGSZ are sporadically well developed throughout the eastern half of the CMB (Fig. 5b). The SGSZ has deformed the north-striking mafic dykes of the Marnda Moorn large igneous province (Fig. 6e), indicating that the former was active after c. 1200 Ma (although it may also have had an older shearing history).

The Lady Springs Shear Zone (LSSZ) manifests as an anastomosing network of sinistral strike-slip shear zones with predominant constrictional fabrics (L>S to pure L tectonites), in the central–western part of the CMB. This structure is well exposed between Shady Hills and Mogumber, and its southern portion corresponds to the 'Lady Springs shear zone' of Bretan (1985); hence, this name is retained here.

Structures associated with the LSSZ are exposed only in the western half of the CMB and comprise mylonites and mylonitic gneisses with a prominent subhorizontal stretching and mineral lineation (Fig. 6f). Conventional shear sense indicators such as S–C and C' fabrics, and mantled porphyroclasts with monoclinic symmetry, reveal a consistent sinistral shear sense (Fig. 6f,g). L>S and L tectonites occur in all lithologies sheared along the LSSZ, and there is commonly a sharp transition between the two fabrics, at the metre- to decimetre scale, with mutual crosscutting relationships (Fig. 6h–j).

Presumed Proterozoic folds occur throughout the CMB, associated with both the SGSZ and LSSZ. They are particularly common (easier to detect) in well-layered rock types, such as the migmatites and the layered granitic schists. We distinguish between mylonitic (syn-metamorphic) and postshearing (post-metamorphic) folds. Mylonitic folds are typically found along the high-strain zones and are dominated by isoclinal and sheath folds (Fig. 7a,b). Spectacular examples are well exposed in layered granitic schist along the Avon River, between Bells Rapids and Syd's Rapids (Fig. 7b,c). Isoclinal folds were also sporadically observed in non-layered rocks (Fig. 7d), although their recognition might be hampered by the lack of prominent markers (i.e. layering). The mylonitic folds typically have axial planes parallel with the local shear fabric; hence, they are generally upright (i.e. have subvertical axial planes) and have fold axes subparallel to the local mineral or stretching lineation (Fig. 7e); so are typically steeply south-plunging (Fig. 7a–d), or subhorizontal (Fig. 7f) if associated with the SGSZ or the LSSZ, respectively. Many folds are associated with discrete, metre-scale shear zones that probably developed to accommodate strain during folding (Fig. 7g).

Post-shearing folds clearly postdate the main shearing events and associated metamorphism because they deform gneissic to mylonitic foliation. They are typically disharmonic with irregular wavelength and amplitude (Fig. 7h) and exhibit north-striking, steep axial planes, with no axial planar fabric, and axes with variable orientations. These younger folds may have developed during the latest stages of the shearing event that generated the mylonitic folds, or they may be part of unrelated, younger deformation events.

We have not used fold geometry to independently validate shear sense determined using other criteria, regarding them to be unreliable because apparent shear sense can be reversed along fold limbs, depending on the relative timing between the development of folds and pervasive shear fabric, as well as on the angle between the lineation and the fold axis (Goscombe and Trouw, 1999).

Archean structures and fabrics

Several lines of evidence suggest that shearing preserved in the migmatitic structures throughout the CMB (Fig. 8a) are of Archean age. In the first instance, clusters and swarms of migmatite xenoliths are common within the Archean leucogranites of the Darling Range Batholith that intruded the CMB at c. 2626 Ma (Nemchin and Pidgeon, 1997); however, migmatitic structures do not occur in the granitic rocks themselves (as previously noted by Wilde and Low, 1975; Fig. 8b). Representative examples occur a few hundred metres east of the SGSZ, within the Avon River, where swarms of migmatite xenoliths highlight the east-striking magmatic foliation in the leucogranite (Fig. 8b); showing, therefore, a magmatic fabric of Archean age, which is completely devoid of post-Archean tectonic overprint. Furthermore, high-strain fabric in migmatites contained in the CMB is locally cut by undeformed pegmatites and aplites, which are likely part of the Darling Range Batholith (Fig. 8c). In the hills east of the Darling Scarp, between Armadale and Keysbrook, about 30–60 km south of the southern extent of the CMB (asterisk in Fig. 1), extensive exposures of north-striking, subvertical, layered granitic migmatites are intruded by concordant granitic sheets belonging to the Darling Range Batholith that are devoid of any solid-state fabric; therefore, must postdate migmatite shearing (Fig. 8d). Migmatites and granites here were subsequently intruded by a dense array of invariably

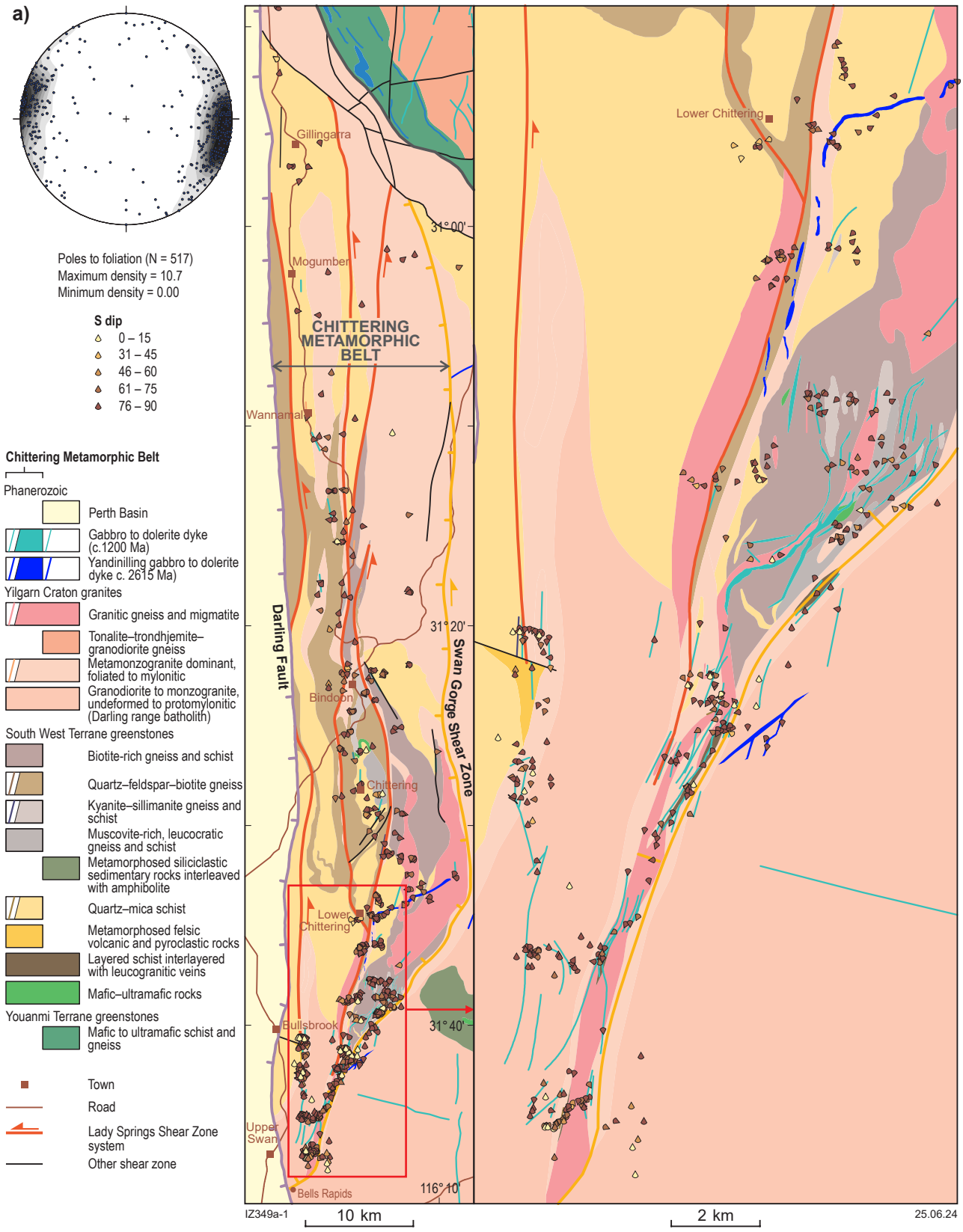

Figure 5. Geological map and structural data of the Chittering Metamorphic Belt: a) map distribution of foliation measurements, colour-coded as a function of the foliation dip value. The corresponding distribution of foliation poles in the equal-area projection plot is shown at left. On average, the regional foliation dips steeply to the west, subparallel to the Darling Fault.

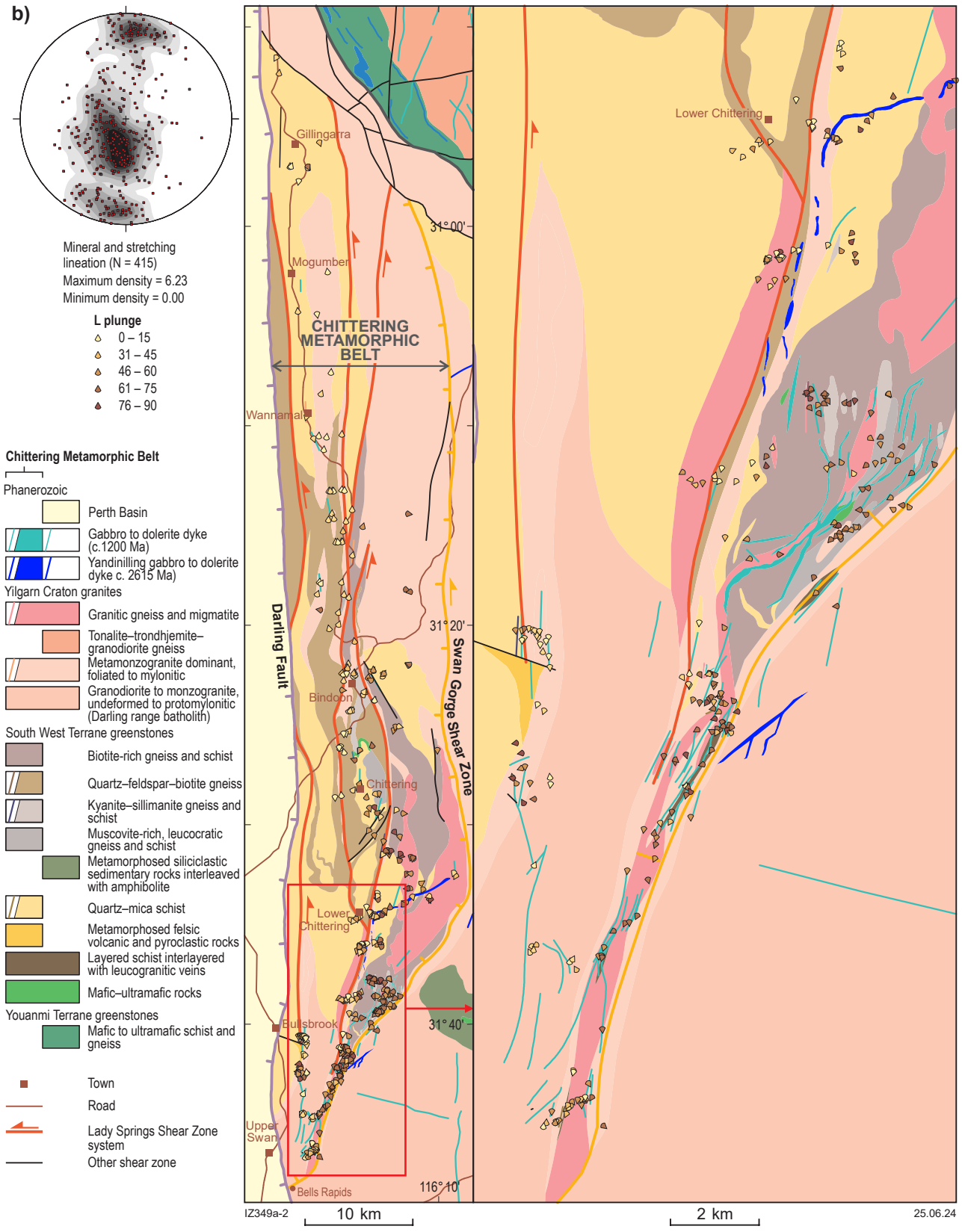

Figure 5. (continued) b) map distribution of stretching and mineral lineation measurements, colour-coded as a function of the lineation plunge value. The corresponding distribution of stretching and lineation in the equal-area projection plot is shown at left. Steep plunges occur along the SGSZ; whereas, the LSSZ is associated with subhorizontal linear fabrics.

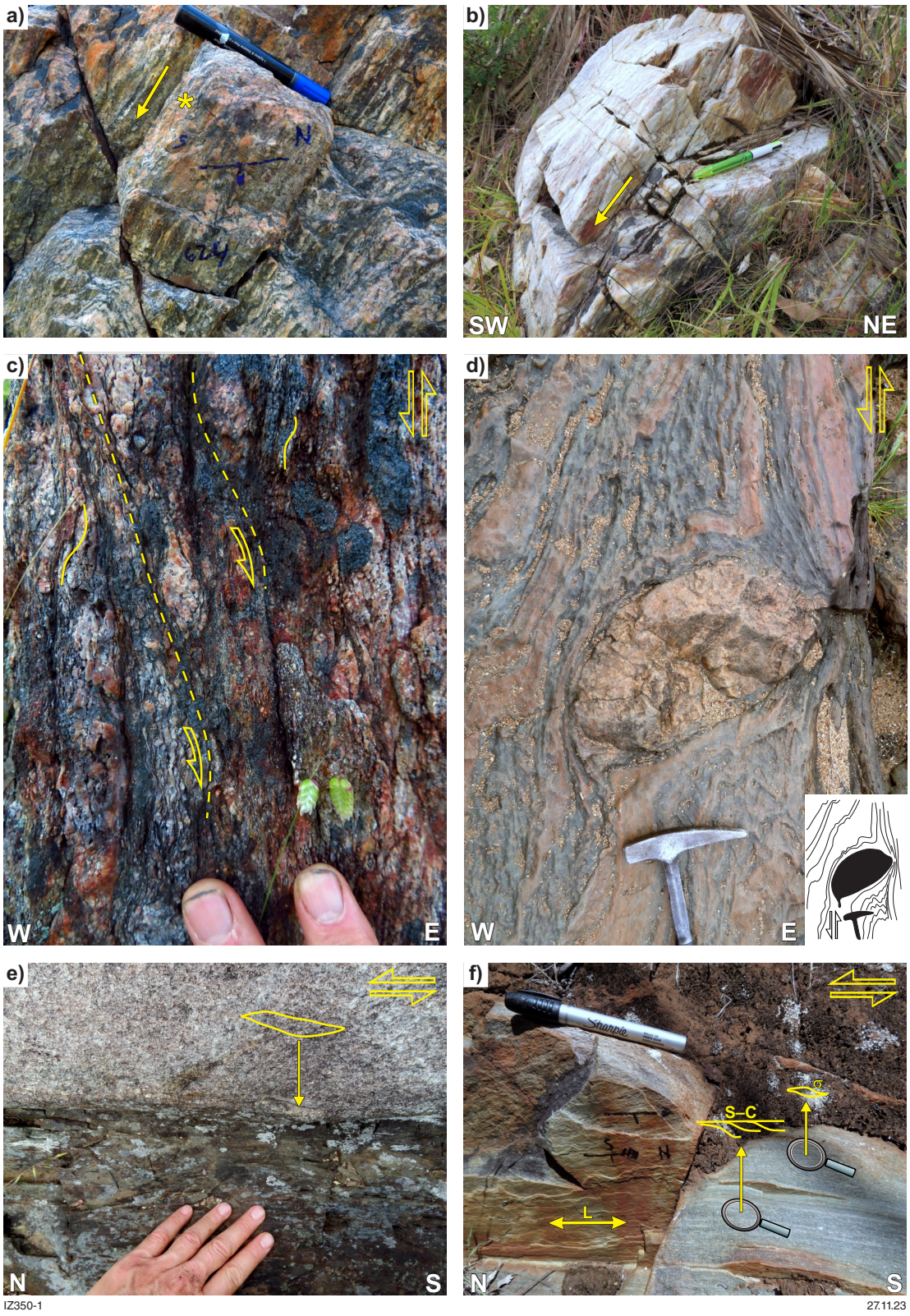

Figure 6. Typical outcrop-scale geometry, kinematics and shear sense indicators mapped along the Swan Gorge (a–e) and the Lady Springs (f–l) shear zone systems: a) foliation-parallel view of sheared granitic migmatite, exposed along the southern end of the study area. The arrow is parallel to the stretching lineation. The asterisk marks the approximate location of c); b) three-dimensional view of a sheared quartz vein along the Avon Valley, near Bells Rapids. The arrow is parallel to the stretching lineation; c) close-up view of the area marked with an asterisk in a). C' shear bands indicate sinistral/west-side-down kinematics; d) sheared layered granitic schists exposed along the Swan River. A sigmoidal granitic clast, likely representing the remnants of a boudinaged dyke, indicate sinistral/west-side-down kinematics; e) sheared contact between a c. 1200 Ma dolerite dyke (at bottom) and the host granite of the Darling Range Batholith, exposed near Brigadoon. Sigmoidal foliation indicates sinistral/west-side-down kinematics; f) three-dimensional view of mylonitic two-mica equigranular granite. The foliation-parallel (vertical) exposure shows the subhorizontal stretching lineation; whereas, on the adjacent horizontal exposure, S–C fabric and sigmoidal feldspar porphyroclasts point to sinistral shear sense

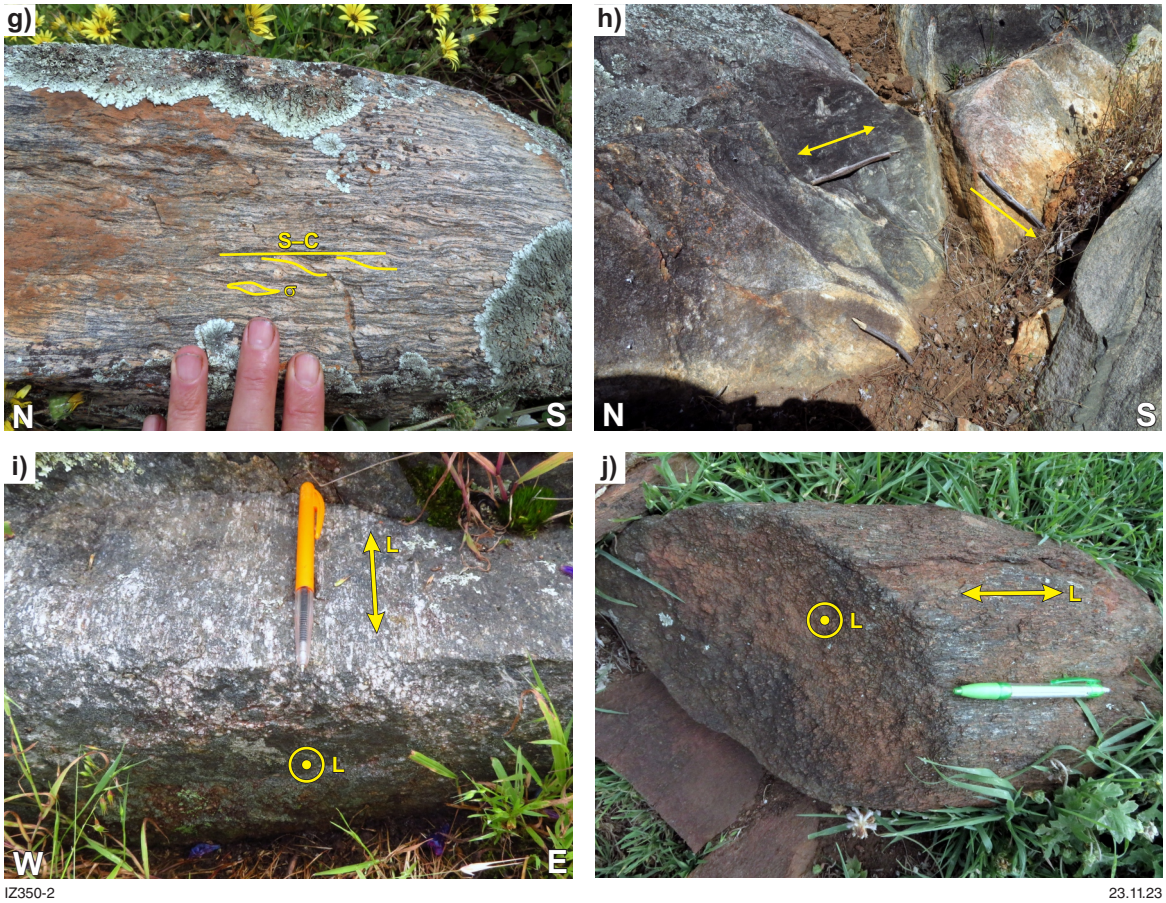

Figure 6. (continued) g) mylonitic gneiss after porphyritic granite. S–C fabric and sigmoidal feldspar porphyroclasts point to sinistral shear sense; h) contact between grey–blue mylonitic, two-mica, equigranular granite and coarse-grained leucogranitic gneiss. The arrows point to the contrasting lineation orientation in the adjacent layers; i) Ltectonite from two-mica tonalite exposed along the Chittering Valley. Note the virtual absence of foliation on the vertical exposure; j) Ltectonite after a dolerite dyke, exposed along the Chittering Valley.

undeformed gabbro to dolerite dykes. These observations indicate that shearing in the Armadale–Keysbrook area is older than c. 2626 Ma, i.e. the minimum age of the Darling Range Batholith (Nemchin and Pidgeon, 1997) and, therefore, that the steep, north-striking orientation of the regional shear fabric in the migmatites is an Archean feature.

Brittle structures and low-temperature shear zones

The Darling Fault is a c. 1500 km long, north-striking, steeply west-dipping structure that was active during the Permo–Cretaceous rifting and breakup of eastern Gondwana (Song and Cawood, 2000). In its hanging wall, the Perth Basin formed initially as an intracontinental rift and evolved into a passive margin along southwestern Australia when Greater India moved away from Australia (Song and Cawood, 2000). The majority of structural investigations of the Perth Basin have been performed using geological, seismic, gravity, magnetic and digital elevation data from the basin itself (Song and Cawood, 2000; Olierook et al, 2015; Thomas, 2018), and there has been little attention dedicated to associated structures in the footwall of the fault along the Darling Scarp.

Most brittle structures and low-temperature shear zones occur within approximately three kilometres from the craton-scale Darling Fault, in the westernmost CMB. Spatial proximity suggests a genetic relationship; that is, most of these brittle footwall structures developed during shearing along the Darling Fault (although the occurrence of Precambrian low-temperature shear zones cannot be ruled out *a priori*). Low-temperature shear zones mapped in the western CMB exhibit outcrop-scale features such as knifesharp faults and complex networks with damage zones that can be several metres thick. Most recognized low-temperature shear zones are north-striking and subvertical, i.e. subparallel with the Darling Fault (Fig. 9), but there are examples that are spatially associated with gabbro–dolerite dykes and are at a high angle to the Darling Fault which may have developed during dyke emplacement, or be due to reactivation of appropriately oriented intrusive contacts.

Many of the north-striking, low-temperature structures clearly play an important role in controlling the topography of the Darling Scarp (Fig. 10a), suggesting that they represent the youngest shearing event in the area, so are probably of Cretaceous age. Slickenlines and stretching lineations vary from steeply plunging with mostly west-side-down movement, to subhorizontal (Fig. 9; Fig. 10b–d), with either dextral or sinistral strike-slip-dominated shear

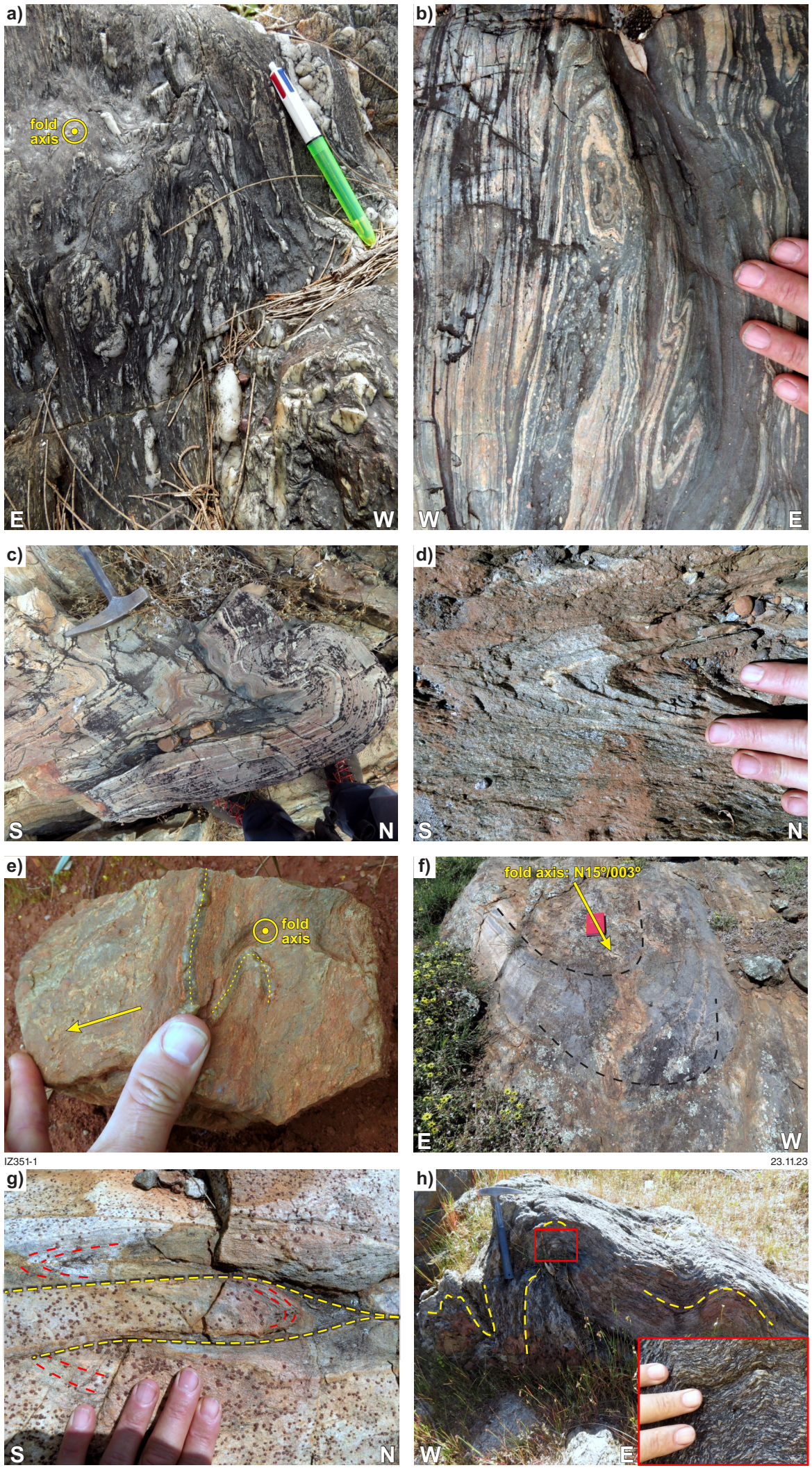

Figure 7. Typical outcrop-scale appearance of folds exposed throughout the CMB, distinguished between mylonitic folds (a–g) and post-mylonitic folds (h): a) sheared and folded quartz veins, intruded into granitic migmatites exposed at Bells Rapids. Fold axes are steeply south plunging; b) isoclinal and sheath folds in layered granitic schists exposed along the Avon Valley, near Syd's Rapids. Fold axes are steeply south plunging; c) subvertical fold in layered granitic schists exposed along the Avon Valley. Disharmonic, contorted folds are likely the result of strain accommodation between layers with different thickness; d) isoclinal fold in two-mica tonalitic gneiss. Fold outline is evidenced by ptygmatic folds in a millimetre-thick aplite vein; e) hand sample of a sheared dolerite dyke associated with folded quartz veins. The three-dimensional view shows that the fold axis is subparallel to the lineation (parallel to the arrow), marked by stretched plagioclase porphyroclasts and aligned amphibole grains; f) meter-scale, subhorizontal isoclinal fold developed in amphibole-bearing tonalitic migmatite gneiss, exposed along the LSSZ; g) isoclinal folds in garnet–biotite migmatitic schist exposed along the LSSZ. Discrete, millimetre-thick shear zones (marked by the broken lines), associated with quartz veins, occur along the limbs of the isoclinal folds; h) disharmonic, plurimetric and upright folds in two-mica, kyanite–sillimanite quartz schist, exposed at Bindoon Hill. The inset at lower right shows a close-up view of the hinge zone, showing the crenulation of the metamorphic foliation, and locality of the kyanite crystals. Note the lack of any visible axial-planar fabric.

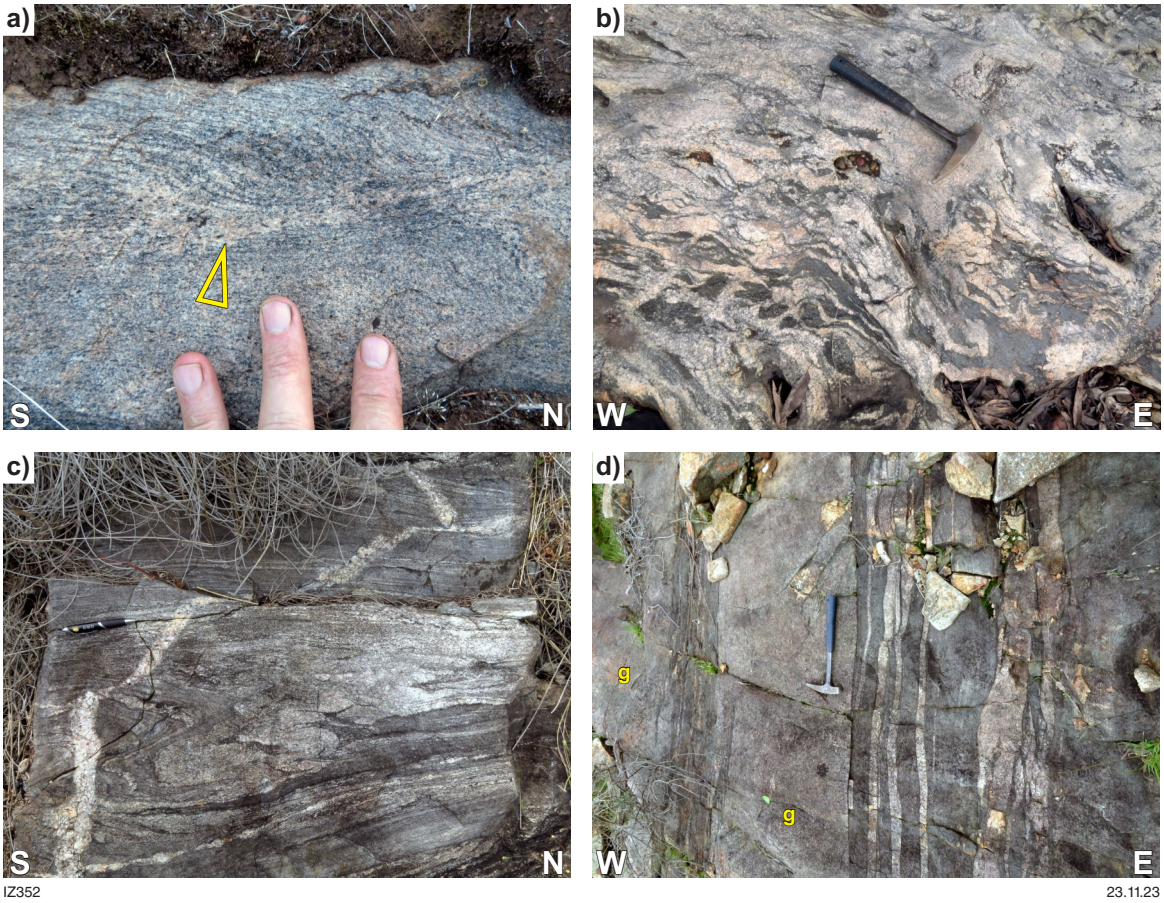

Figure 8. Representative migmatitic structures preserved within the CMB and in the host granites of the Darling Range Batholith: a) Foliated granitic migmatite exposed in the Chittering Valley. The arrowhead points to a leucosomes vein injected along a small-scale sinistral shear band, which is associated with sigmoidal foliation. Note the diffuse and irregular margins of the leucosome, which indicate that it was produced locally; b) train of migmatite xenoliths highlighting the eaststriking magmatic foliation in the host leucogranite, exposed along the Avon Valley, about 500 m east from the SGSZ; c) subvertical isoclinal and ptygmatic folds in high-strain, amphibolebearing tonalitic migmatite gneiss. The shear fabric is postdated by an undeformed pegmatite; d) layered granitic migmatite exposed on the Armadale Hills. Migmatite is intruded by concordant, tabular leucogranite sheets (g) that preserve pristine magmatic fabric.

sense (Fig. 10e–g). Many low-temperature structures show superposition of both movement types, implying either progressive deformation during a single shearing event, or distinct shearing episodes separated by periods of tectonic quiescence.

Low-temperature ductile shear zones are also common, characterized by mantled feldspar porphyroclasts and plastically deformed quartz lenses (probably remnants of boudinaged quartz veins, Fig. 10e–g). The very sharp boundaries of some of these ductile shear zones (Fig. 10f) and the sporadic occurrence of cataclasite pockets along them (Fig. 10g,h) suggests that these mylonites nucleated on brittle precursors (Mancktelow and Pennacchioni, 2005). Other structures show converse evolution, from relatively broad ductile shear bands, to more localized brittle structures (Fig. 11), likely reflecting cooling and/or an increase in strain rate during a single shearing event.

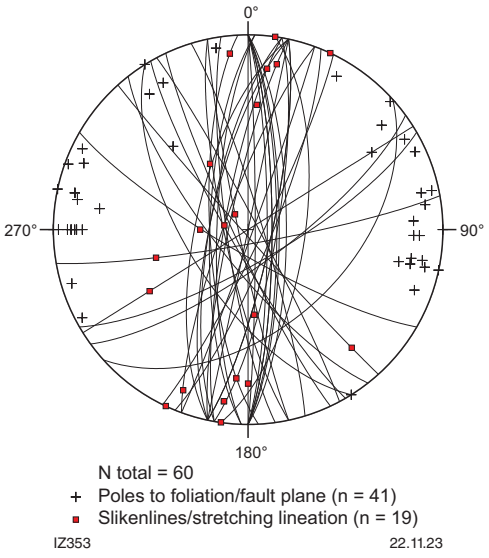

Figure 9. Equal-area plot of planar and linear structures associated with low-temperature shear zones and faults, exposed along the western margin of the CMB.

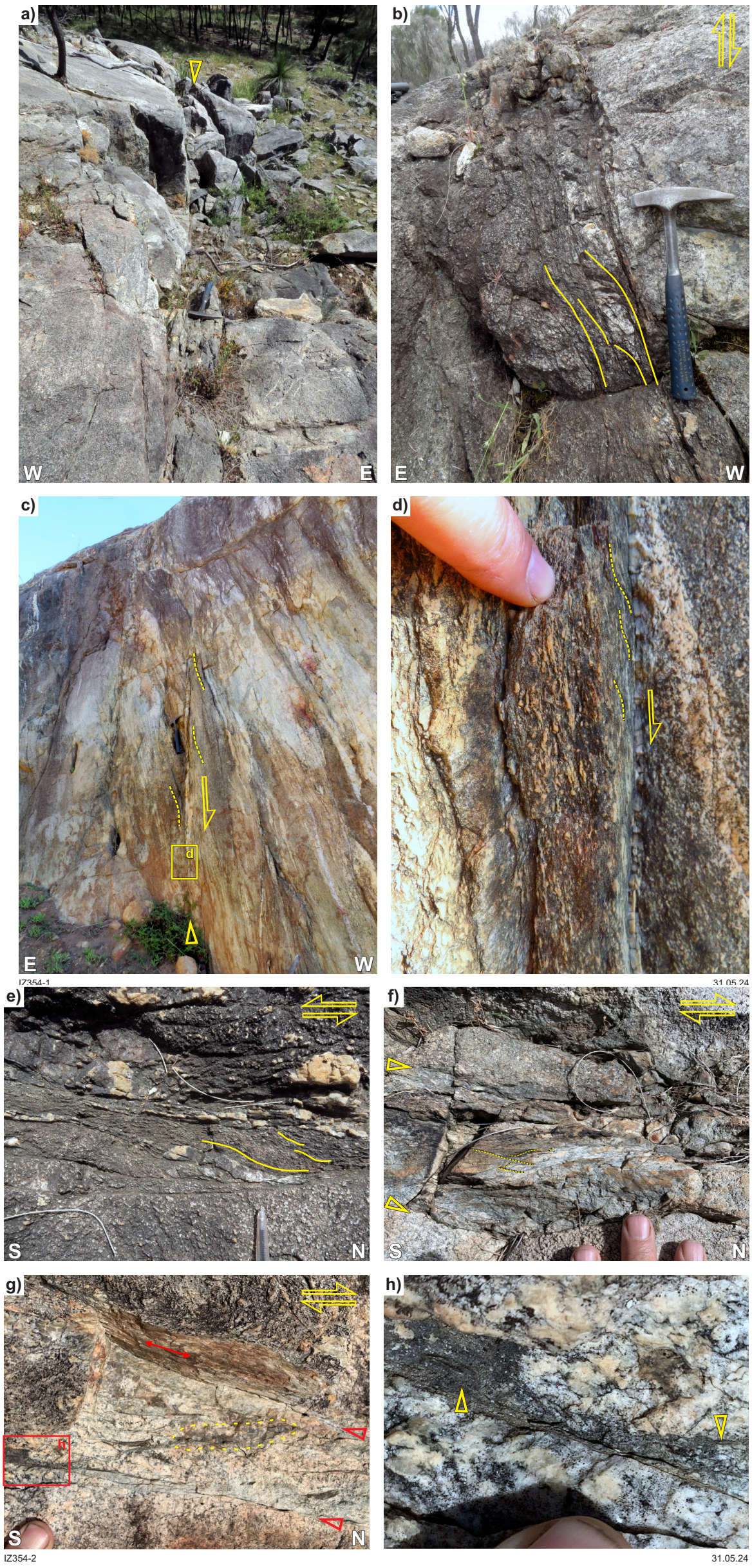

Figure 10. Typical outcrop-scale appearance of faults and low-temperature shear zones exposed in leucogranite, along the western margin of the CMB, within the Walyunga National Park: a) northstriking sinistral strike-slip fault (whose trace is indicated by the arrowhead) exposed in leucogranite. Note that the fault controls the morphology of the large granite outcrop, and its erosion; b) vertical exposure of the same outcrop shown in a), view approximately indicated by the arrowhead shown in a). S–C fabric in foliated cataclasite suggests the existence of a component of normal (west-side-down) kinematics; c) subvertical exposure of leucogranitic gneiss exposed near Bullsbrook. The steeply west-dipping gneissic fabric is truncated by a narrow, sharp shear zone that dips 85° to the west. The deflection of layering along the shear zone (broken lines) indicates normal kinematics. The box shows the location of d); d) close-up view from the outcrop shown in c), showing that the narrow shear zone is associated with a millimetrethick quartz vein. Sigmoidal foliation (broken lines) indicates normal kinematics; e) horizontal close-up view from the fault shown in a). S–C fabric, highlighted by sheared and boudinaged quartz veins, indicates sinistral shear sense; f) subhorizontal exposure from a lowtemperature, narrow shear zone, highlighted by boudinaged quartz veins, within a finegrained greenish matrix. S–C fabric indicates dextral shear sense. The knife-sharp shear zone boundaries (arrowheads) against the undeformed leucogranite suggest that the ductile shear zone nucleated on a brittle precursor; g) another exposure of the shear zone shown in f). The sharp boundaries against the undeformed leucogranite (arrowheads) contain discontinuous layers and pockets of cataclasite. A ductile component of shearing is indicated by the plastically sheared quartz lens (contoured by the yellow broken line). The double arrow points to the subhorizontal orientation of slickenlines, visible on the small subvertical exposure. The red box shows the location of h); h) close-up view from g), showing the millimetre-sized cataclasite pockets (arrowheads) that decorate the knife-sharp fault surface.

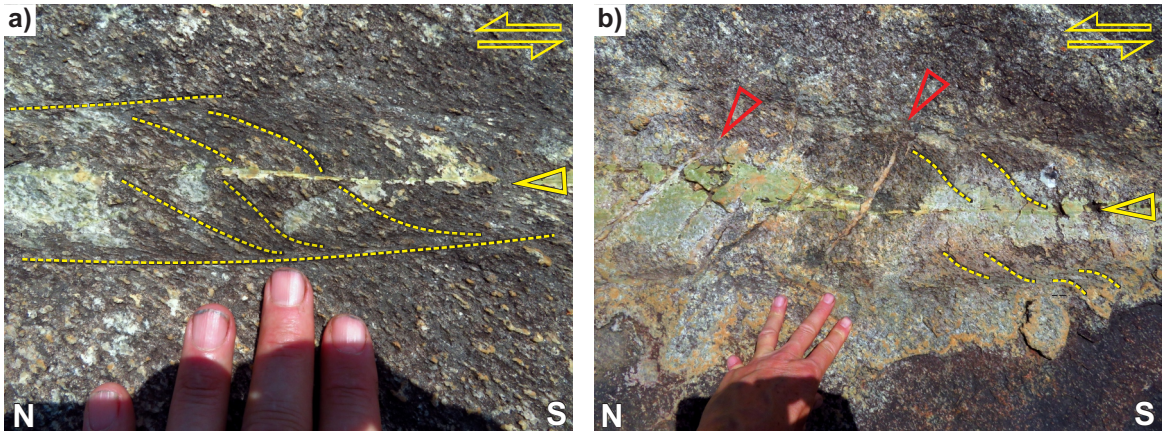

Figure 11. Representative example of brittle structures developed on a ductile precursor in leucogranite: a) the S–C fabric in a centimetre-thick sinistral shear zone is transected by an epidote-decorated, knife-sharp fault (arrowhead), which developed along the median line of the shear zone; b) close-up view on another portion of the shear zone shown in a), demonstrating that both ductile and brittle structures are postdated by a set of tension gashes (red arrowheads), whose orientation is consistent with the overall sinistral sense of shear. The yellow arrowhead points to the same fault shown in a).

Microstructures and quartz crystallographic preferred orientations

Microstructures

Proterozoic ductile fabrics

Microfabrics in the samples collected from Proterozoic ductile shear zones range from relatively low-strain gneissic to ultramylonitic. Low- to moderate-strain gneissic fabrics in meta-igneous rocks are relatively coarse-grained, with millimetre-to-centimetre-sized feldspar porphyroclasts wrapped by coarse-grained quartz ribbons and mica flakes (Fig. 12a). Quartz grain boundaries are deeply sutured, suggesting recrystallization predominantly via grain-boundary migration, at temperatures in excess of ~500 °C (Stipp et al, 2002), assuming normal strain rates and water activity. Quartz–feldspar phase boundaries are typically deeply lobate (Fig. 12a), which indicates diffusion creep at a temperature close to the granite solidus (Gower and Simpson, 1992), hence deformation of crystallizing granites or partially melting migmatitic rocks. Gneissic rocks with higher strain fabrics (Fig. 4a) show partial recrystallization of feldspar phenocrysts to finer grained (<400 µm) aggregates (Fig. 4b), suggesting shearing at amphibolite-facies conditions (Tullis and Yund, 1987; Rosenberg and Stünitz, 2003).

Quartz grain boundaries in quartz-rich schists are deeply sutured, suggesting recrystallization predominantly via grain-boundary migration at temperatures exceeding ~500 °C (Stipp et al, 2002). Accessory poikiloblastic kyanite grains that define the lineation in outcrop (Fig. 4i) include the recrystallized quartz-rich matrix (Figs 4h, 12b), suggesting a synkinematic origin (Passchier and Trouw, 2005). Kyanite is commonly replaced by sigmoidal aggregates of fibrolite along microscale shear zones (Fig. 12c), that must have developed at temperatures in excess of ~500 °C, i.e. the minimum temperature for the kyanite–sillimanite phase transition, (Vernon, 2004).

Generally, ductile shearing of quartz-rich schists under retrograde metamorphic conditions led to cataclastic deformation of kyanite and sillimanite, and their partial-to-total replacement by synkinematic muscovite (Fig. 12d). Retrograde fabrics in granitic gneisses (*sensu lato*) are characterized by dominant subgrain-rotation recrystallization in quartz and low-temperature plasticity in feldspars (Simpson, 1985), suggesting fabric development at temperatures in the range of 400–500 °C (Stipp et al, 2002). The fabric intensity can vary from protomylonitic (Fig. 12f), to mylonitic (Fig. 4f), to ultramylonitic (Fig. 12g), with increasing finite strain.

Archean ductile fabrics

There are numerous locations where outcropping rocks show macroscopic evidence of meltpresent deformation (Fig. 8a). Microstructures in samples from such domains are typical for rocks that were deformed at near-solidus temperatures, including chessboard subgrain boundary patterns in quartz (Fig. 13a) – reflecting its deformation at hightemperature, in the high-quartz field (Kruhl, 1996) – and deeply lobate quartz–feldspar phase boundaries with feldspar cusps parallel with the foliation (Fig. 13a,b), indicating the occurrence of diffusion creep at temperatures close to the granite solidus during the shearing event that generated the main fabric (Gower and Simpson, 1992; Rosenberg and Stünitz, 2003). Recrystallization of high-strain samples at high temperature is indicated by a bimodal feldspar grain-size distribution, in which millimetre-sized porphyroclasts are accompanied by aggregates of smaller (<200 µm), recrystallized grains (Fig. 13b; Tullis and Yund, 1991; Rosenberg and Stünitz, 2003). Several rock units preserve remnants of high-temperature microstructures variably overprinted by Proterozoic ductile fabrics, testifying that the older shear fabrics may have been originally much more widespread.

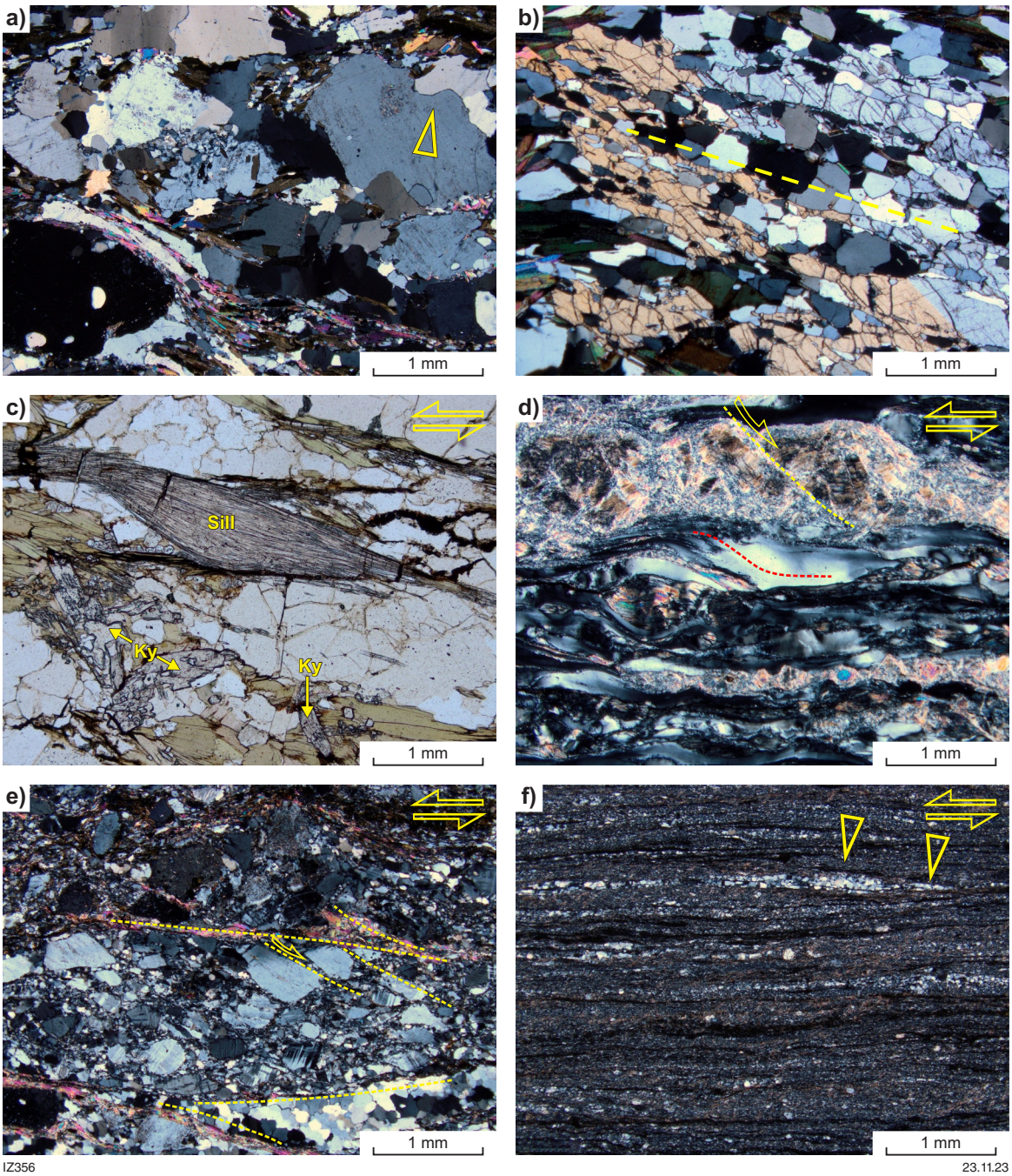

Figure 12. Representative microstructures from the samples collected along Proterozoic shear zones: a) gneissic microfabric in two-mica tonalitic gneiss, with foliation marked by mica flakes and elongate, coarse-grained quartz aggregates. The arrowhead points to a lobate quartz–plagioclase phase boundary; b) poikiloblastic kyanite in quartz schist from Bindoon Hill. The blast included the foliated matrix (the broken line marks the foliation trace); c) millimetre-thick shear zone in quartz schist, showing development of sigmoidal sillimanite aggregates at the expense of kyanite (Ky). Plane polarized light; d) high-strain, retrograde fabric in quartz schist. Kyanite experienced brittle deformation (the broken yellow line marks an antithetic microfault) and partial replacement by muscovite. The red broken line highlights the sigmoidal shape of stretched quartz porphyroclasts, whose shape is consistent with sinistral shear sense; e) retrograde mylonitic fabric in granitic gneiss. Broken lines highlight the S–C surfaces that define the sinistral shear sense. Angular feldspar porphyroclasts are wrapped by fine-grained recrystallized albite. The arrow indicates an antithetic microfault in a K-feldspar porphyroclast; f) granitic ultramylonite from the outcrop shown in Fig. 6f. The quartz–albite–mica fine-grained matrix wraps around remnants of feldspar porphyroclasts that do not exceed 100 μm in size. The arrowheads point to the sigmoidal shape of quartz ribbons, which define the sinistral shear sense.

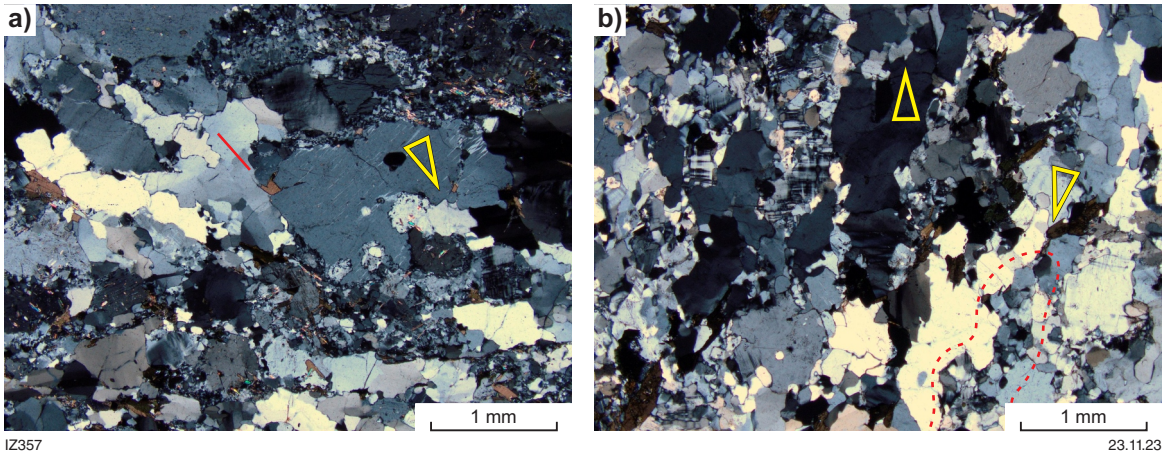

Figure 13. Microstructure from samples preserving outcrop-scale evidence of melt-present deformation: a) low-strain granitic migmatite showing intensely lobate margins (arrowhead) between K-feldspar and quartz. Quartz here typically shows two sets of mutually perpendicular subgrain boundaries, which are parallel and perpendicular to the c-axis (whose trace is indicated by the red line); b) higher-strain version of granitic migmatite, showing widespread feldspar recrystallization (one example is circled by the red broken line), and deeply cuspate–lobate feldspar–quartz boundaries. Note that feldspar cusps (arrowheads) consistently point to the foliation trace.

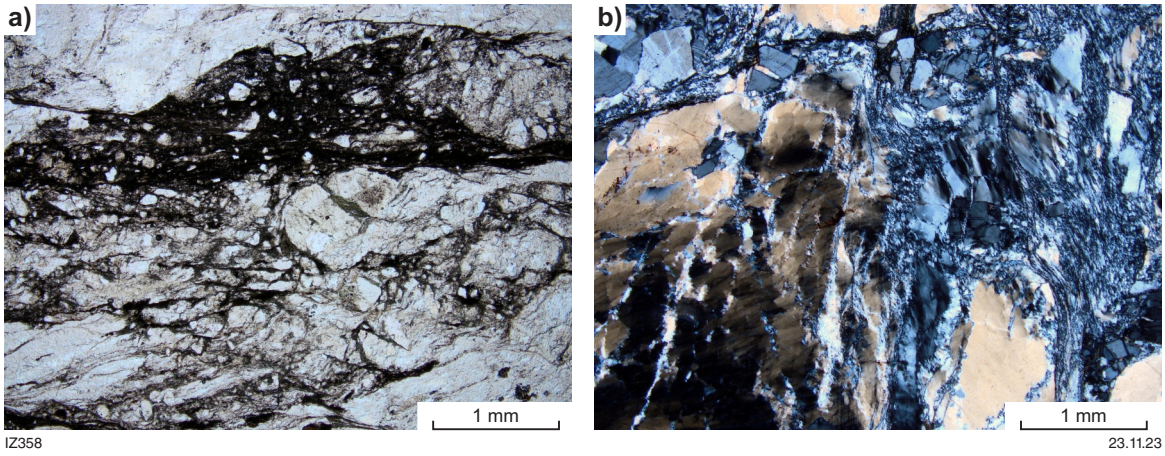

Figure 14. Typical microstructures from low-temperature shear zones: a) microstructure from the cataclasite shown in Fig. 10h. Angular granite fragments of variable size are included in an ultrafinegrained matrix, likely mostly composed of illite. Plane polarized light; b) microstructure from the sheared quartz vein shown in Fig. 10g. The large quartz porphyroclasts show widespread undulose extinction and are transected by narrow shear bands. Note that, particularly in the upper-right corner of the micrograph, several quartz porphyroclasts have angular shape.

Brittle structures and low-temperature shear zones

Cataclastic shear zones in leucogranite of the Darling Range Batholith show angular clasts of variable size supported in an ultrafine-grained matrix (Fig. 14a). Where lowtemperature ductile shear zones have nucleated on a brittle precursor (Fig. 10c), there is widespread recrystallization of quartz into fine-grained aggregates (10–50 µm: Fig. 14b). Quartz porphyroclasts show irregular but generally intense undulose extinction and are transected by narrow shear bands (Fig. 14b), a microstructure suggesting deformation mainly via bulging recrystallization close to the quartz brittle–ductile transition at temperatures of 350–400 °C (Stipp et al, 2002). The angular shape of several quartz porphyroclasts probably derives from the early stage of cataclastic deformation (i.e. compare Figure 14a with 14b).

Quartz crystallographic preferred orientation (CPO) data

CPO investigations have proven to be powerful in unravelling the structural evolution of complex terranes, since they can provide important constraints about the dominant shear sense, deformation temperature and type of bulk flow; that is, flattening, constriction or plane flow (Law, 2014). During deformation, mineral CPO usually develops mainly through dislocation creep processes, where crystals are deformed along one or more slip systems which are typical for each mineral. The type of slip systems that are active in a crystal depends on metamorphic and deformation conditions. As each slip system produces a typical pattern (when data are plotted on stereographic projections), CPO data can be used to infer metamorphic and deformation conditions.

In stereograms, standard presentation of CPO patterns is on north–south axes. This implies that the corresponding foliation and lineation are presented in the diagram as an easterly striking vertical plane and horizontal line respectively, the latter indicated by dots on the circle. CPO patterns are interpreted in terms of their internal and external asymmetry. Internal asymmetry is defined by the shape of the pattern itself; external asymmetry is determined with respect to a reference frame, which typically corresponds to foliations and lineations. Quartz is one of the most common minerals in felsic rocks, and its behaviour during deformation has been studied extensively. Quartz c-axis CPO development has been investigated through both theoretical approaches and through studies of rocks. Given that quartz-rich felsic rocks represent the dominant rock type within the CMB, we have here investigated quartz c-axis CPO fabrics in representative samples from the main generations of fabrics recognized in this work, and also with the aim of obtaining a uniform geographical coverage of the whole CMB.

We have collected and analyzed quartz CPO data from 97 samples (Tab. 3) throughout the CMB (Fig. 15a), following the procedure described by (Zibra and Peternell, 2023). Background details on the rationale and usefulness of CPO data are widely available in the geological literature (Lister and Hobbs, 1980; Schmid and Casey, 1986; Passchier and Trouw, 2005; Hunter et al, 2018). Figure 15b provides the essential information to allow the reader to interpret quartz CPO data presented here.

Seventeen samples (assigned here to group A) exhibit maxima at a low angle from the stretching lineation, which is indicative of dominant prism <c> slip, reflecting shearing at near-solidus temperatures (Mainprice et al, 1986; Stipp et al, 2002), in the high-quartz field (Kruhl, 1996). These maxima are locally prominent (GSWA 250659, 250681, 250682, 250694 and 251224; Fig. 16) but are more commonly associated with additional maxima located near the y-axis (i.e. near the centre of the plot), or near the z-axis, normal to the foliation (Fig. 16). These additional maxima are indicative of activation of prism <a> slip and basal <a> slip, respectively. We interpret them to reflect variable degrees of lower temperature overprint of the earlier high-temperature migmatitic fabrics, consistently with the observed meso- and microstructures. Nine of these 17 samples show an external monoclinic symmetry, i.e. with respect to the foliation and lineation in the sample (Bouchez et al, 1983), which indicate dominant non-coaxial deformation and sinistral shear sense, consistently with the observed structures (Fig. 8a). These high-temperature fabrics are preserved locally, at various locations throughout the CMB, typically in the low-strain domains with respect to the main Proterozoic shear fabrics (Fig. 15a).

Twenty samples show a prominent maximum near the y-axis, which is, in places, accompanied by a weakly-developed girdle pattern normal to the foliation (Fig. 17). Collectively, we refer to them as group B samples. This fabric type typically indicates dominant prism <a> slip at amphibolitefacies conditions (Schmid and Casey, 1986; Passchier and Trouw, 2005). In eight of these samples, the girdle pattern has a long axis normal to the foliation plane (Fig. 17), reflecting dominant coaxial deformation (Bouchez et al, 1983; Passchier and Trouw, 2005; Hunter et al, 2018). In the remaining eight samples of this group, the long axis of the girdle is oblique to the foliation plane, suggesting dominant non-coaxial deformation and sinistral shear sense in seven samples (Fig. 17). Samples with such prominent maxima along the y-axis are mainly located along the major Proterozoic shear zones (Fig. 15a), indicating that they developed – at least in part – under amphibolite-facies conditions. These results are in agreement with the occurrence of synkinematic sillimanite (Fig. 12c), which suggests a minimum temperature of about 500 ºC for the onset of shearing along these structures.

The majority of the analyzed samples (n=53, assigned here to group C) show quartz CPO patterns that transition from single girdle with well-developed near-y maxima, to patterns showing prominent maxima in near-z position (normal to the foliation, Fig. 18). Girdle patterns at high angle to the foliation reflect the activation of prism <a> slip, together with basal <a> slip and rhomb <a> slip, with the latter contributing to produce maxima in intermediate position between the y-axis and the z-axis (Fig. 15b). Quartz CPO patterns dominated by near-z maxima, reflect prevailing basal <a> slip at greenschist facies conditions (Passchier and Trouw, 2005). Overall, group C samples show a gradual transition with the group B samples (with the latter showing single, prominent maxima near the y-axis; compare Figs 17, 18). Furthermore, group C samples are mainly located along the same major Proterozoic shear zones from which the group B samples come from (Fig. 15a). These data, in agreement with the observed microstructures, suggest that the onset of shearing along Proterozoic shear zones occurred under amphibolite-facies conditions followed by retrograde shearing down to greenschist-facies conditions. Comparable quartz CPO results were obtained by Bretan (1985), but with a dominance of girdle-type fabrics (equivalent to the group B samples presented here), since Bretan targeted the highest-strain domains of both the SGSZ and LSSZ, in which retrograde fabrics are generally well developed.

Seven samples show diffuse quartz CPO patterns with maxima scattered throughout the plot (Fig. 19). Most of these samples show sub-maxima close to the y-axis and z-axis, and in intermediate positions. These patterns likely reflect a combination of superposed fabrics and/or the occurrence of non-quartz phases that may have weakened the overall fabric (Hunter et al, 2019).

Table 3. List of GSWA samples analyzed for quartz c-axis CPO.

Sample ID	Site ID	Quartz CPO fabric type	Lithname	structural domain	Latitude	Longitude
237099	IXZWOO0000001	Y max - non coaxial	granitic gneiss	SGSZ	-31.773	116.062
237100	IXZWOO0000001	Y max - non coaxial	granitic gneiss	SGSZ	-31.773	116.062
250610	IXZWOO0000009	X max - non coaxial	granitic gneiss	SGSZ	-31.778	116.068
250613	IXZWOO0000012	Y max - coaxial	granitic gneiss	SGSZ	-31.773	116.063
250614	IXZWOO0000013	Y max - coaxial	granitic gneiss	SGSZ	-31.772	116.064
250615	IXZWOO0000014	Y max - non coaxial	granitic gneiss	LSSZ	-31.767	116.06
250617	IXZWOO0000016	Y max - non coaxial	quartz vein	SGSZ	-31.775	116.057
250620	IXZWOO0000019	single girdle - non coaxial	granitic gneiss	Darling Scarp	-31.742	116.053
250622	IXZWOO0000020	single girdle - non coaxial	granitic gneiss	SGSZ	-31.745	116.061
250623	IXZWOO0000021	Y max - coaxial	granitic gneiss	LSSZ	-31.744	116.061
250624	IXZWOO0000022	Y max - non coaxial	mylonitized metagranitic rock	SGSZ	-31.743	116.067
250627	IXZWOO0000024	Y max - coaxial	granitic gneiss	Darling Scarp	-31.707	116.048
250630	IXZWOO0000027	single girdle - coaxial	granitic gneiss	Darling Scarp	-31.711	116.049
250631	IXZWOO0000028	single girdle - coaxial	granitic gneiss	Darling Scarp	-31.711	116.048
250633	IXZWOO0000030	unclear	kyanite-bearing micaceous gneiss	SGSZ	-31.599	116.115
250634	IXZWOO0000031	single girdle - coaxial	tonalitic gneiss	SGSZ	-31.601	116.118
250635	IXZWOO0000032	single girdle - non coaxial	granitic gneiss	low strain	-31.628	116.114
250637	IXZWOO0000034	unclear	micaceous schist	SGSZ	-31.63	116.124
250638	IXZWOO0000035	X max - non coaxial	migmatitic gneiss	SGSZ	-31.629	116.126
250639	IXZWOO0000035	unclear	migmatitic gneiss	SGSZ	-31.629	116.126
250641	IXZWOO0000037	single girdle - non coaxial	micaceous schist	low strain	-31.63	116.117
250642	IXZWOO0000038	X max - non coaxial	migmatitic gneiss	Archean	-31.63	116.117
250644	IXZWOO0000039	single girdle - coaxial	migmatitic gneiss	LSSZ	-31.6	116.106
250645	IXZWOO0000040	single girdle - coaxial	migmatitic gneiss	LSSZ	-31.6	116.105
250646	IXZWOO0000041	single girdle - non coaxial	granitic gneiss	LSSZ	-31.601	116.104
250648	IXZWOO0000043	single girdle - non coaxial	migmatitic gneiss	LSSZ	-31.601	116.102
250649	IXZWOO0000043	single girdle - non coaxial	migmatitic gneiss	LSSZ	-31.601	116.102
250650	IXZWOO0000044	single girdle - non coaxial	migmatitic gneiss	LSSZ	-31.601	116.101
250651	IXZWOO0000045	X max - coaxial	migmatitic gneiss	SGSZ	-31.602	116.1
250655	IXZWOO0000049	Y max - coaxial	migmatitic gneiss	SGSZ	-31.647	116.086
250656	IXZWOO0000050	single girdle - non coaxial	granitic gneiss	LSSZ	-31.647	116.087
250657	IXZWOO0000050	single girdle - non coaxial	granitic gneiss	LSSZ	-31.647	116.087
250659	IXZWOO0000052	X max - non coaxial	migmatitic gneiss	Archean	-31.64	116.102
250660	IXZWOO0000053	Y max - non coaxial	micaceous schist	LSSZ	-31.607	116.101
250661	IXZWOO0000054	single girdle - coaxial	granitic gneiss	LSSZ	-31.606	116.098
250662	IXZWOO0000055	single girdle - coaxial	migmatitic gneiss	LSSZ	-31.606	116.102
250663	IXZWOO0000056	single girdle - coaxial	micaceous schist	low strain	-31.628	116.109
250664	IXZWOO0000056	single girdle - coaxial	micaceous schist	low strain	-31.628	116.109
250665	IXZWOO0000057	single girdle - non coaxial	migmatitic gneiss	low strain	-31.629	116.108
250667	IXZWOO0000059	unclear	micaceous schist	low strain	-31.632	116.112
250668	IXZWOO0000060	single girdle - non coaxial	quartz-mica schist	low strain	-31.631	116.114
250672	IXZWOO0000065	single girdle - non coaxial	micaceous schist	SGSZ	-31.573	116.089
250674	IXZWOO0000067	Y max - coaxial	micaceous schist	SGSZ	-31.707	116.085
250675	IXZWOO0000068	single girdle - coaxial	micaceous schist	SGSZ	-31.648	116.121
250676	IXZWOO0000069	single girdle - non coaxial	micaceous schist	SGSZ	-31.647	116.12
250676	IXZWOO0000069	unclear	micaceous schist	SGSZ	-31.647	116.12
250677	IXZWOO0000070	single girdle - coaxial	migmatitic gneiss	SGSZ	-31.658	116.115
250678	IXZWOO0000071	single girdle - coaxial	migmatitic gneiss	SGSZ	-31.657	116.117
250679	IXZWOO0000073	X max - coaxial	micaceous schist	low strain	-31.644	116.12
250680	IXZWOO0000074	X max - coaxial	migmatitic gneiss	low strain	-31.645	116.118
250681	IXZWOO0000075	X max - coaxial	micaceous gneiss	low strain	-31.645	116.117
250682	IXZWOO0000075	X max - coaxial	micaceous gneiss	low strain	-31.645	116.117
250683	IXZWOO0000077	X max - coaxial	migmatitic gneiss	low strain	-31.662	116.103
250685	IXZWOO0000079	single girdle - coaxial	micaceous schist	SGSZ	-31.643	116.126
250686	IXZWOO0000080	Y max - coaxial	granitic gneiss	SGSZ	-31.672	116.114
250688	IXZWOO0000081	single girdle - coaxial	micaceous schist	low strain	-31.629	116.112
250689	IXZWOO0000043	single girdle - non coaxial	migmatitic gneiss	LSSZ	-31.601	116.102
250690	IXZWOO0000081	single girdle - non coaxial	micaceous schist	low strain	-31.629	116.112
250691	IXZWOO0000081	single girdle - non coaxial	micaceous schist	low strain	-31.629	116.112
250692	IXZWOO0000081	single girdle - coaxial	micaceous schist	low strain	-31.629	116.112
250693	IXZWOO0000082	Y max - coaxial	granitic gneiss	SGSZ	-31.651	116.126
250694	IXZWOO0000083	X max - non coaxial	micaceous schist	SGSZ	-31.543	116.18
250695	IXZWOO0000085	X max - non coaxial	micaceous gneiss	SGSZ	-31.419	116.13
250696	IXZWOO0000086	single girdle - coaxial	micaceous schist	SGSZ	-31.438	116.166
250697	IXZWOO0000087	Y max - non coaxial	granitic gneiss	SGSZ	-31.63	116.118
250698	IXZWOO0000087	Y max - coaxial	siliciclastic gneiss	low strain	-31.63	116.118
250699	IXZWOO0000088	Y max - coaxial	granitic gneiss	SGSZ	-31.366	116.141
250700	IXZWOO0000089	unclear	granitic gneiss	low strain	-31.24	116.142
251201	IXZWOO0000090	single girdle - coaxial	granitic gneiss	LSSZ	-31.173	116.086
251202	IXZWOO0000091	single girdle - non coaxial	granitic gneiss	LSSZ	-31.374	116.087
251204	IXZWOO0000093	single girdle - coaxial	granitic gneiss	SGSZ	-31.25	116.104
251207	IXZWOO0000096	single girdle - non coaxial	granitic gneiss	LSSZ	-31.178	116.063
251209	IXZWOO0000099	single girdle - coaxial	quartzofeldspathic schist	LSSZ	-30.951	116.058
251210	IXZWOO0000099	single girdle - coaxial	metamorphosed quartz vein	LSSZ	-30.951	116.058
251212	IXZWOO0000101	X max - non coaxial	granitic gneiss	LSSZ	-30.816	116.032
251214	IXZWOO0000103	single girdle - non coaxial	amphibolitic gneiss	LSSZ	-31.071	116.049
251215	IXZWOO0000104	single girdle - non coaxial	granitic gneiss	LSSZ	-31.074	116.065
251216	IXZWOO0000105	X max - coaxial	kyanite-bearing quartz-mica schist	SGSZ	-31.389	116.106
251217	IXZWOO0000106	Y max - non coaxial	granitic gneiss	LSSZ	-31.435	116.085
251218	IXZWOO0000107	single girdle - non coaxial	granitic gneiss	SGSZ	-31.515	116.12
251220	IXZWOO0000056	single girdle - coaxial	micaceous schist	low strain	-31.628	116.109
251221	IXZWOO0000056	X max - non coaxial	micaceous schist	low strain	-31.628	116.109
251222	IXZWOO0000056	unclear	micaceous schist	Darling Scarp	-31.628	116.109
251223	IXZWOO0000056	single girdle - non coaxial	garnet-bearing amphibolite	low strain	-31.628	116.109
251224	IXZWOO0000056	X max - coaxial	garnet-bearing amphibolite	low strain	-31.628	116.109
251225	IXZWOO0000105	X max - non coaxial	kyanite-bearing quartz-mica schist	SGSZ	-31.389	116.106
251226	IXZWOO0000105	single girdle - coaxial	kyanite-bearing quartz-mica schist	SGSZ	-31.389	116.106
251227	IXZWOO0000105	single girdle - coaxial	kyanite-bearing quartz-mica schist	SGSZ	-31.389	116.106
251228	IXZWOO0000105	single girdle - coaxial	kyanite-bearing quartz-mica schist	SGSZ	-31.389	116.106
251229	IXZWOO0000105	single girdle - coaxial	kyanite-bearing quartz-mica schist	SGSZ	-31.389	116.106
251230	IXZWOO0000119	single girdle - non coaxial	granitic gneiss	SGSZ	-31.697	116.092
251231	IXZWOO0000122	Y max - coaxial	granitic gneiss	SGSZ	-31.712	116.083
251233	IXZWOO0000124	single girdle - coaxial	micaceous gneiss	LSSZ	-31.677	116.05
251234	IXZWOO0000125	single girdle - non coaxial	granitic gneiss	LSSZ	-31.677	116.05
251235	IXZWOO0000125	single girdle - non coaxial	siliciclastic schist	LSSZ	-31.677	116.05
251236	IXZWOO0000127	single girdle - non coaxial	metamorphosed quartz vein	Darling scarp	-31.704	116.05
251237	IXZWOO0000126	Y max - coaxial	granitic gneiss	LSSZ	-31.678	116.054

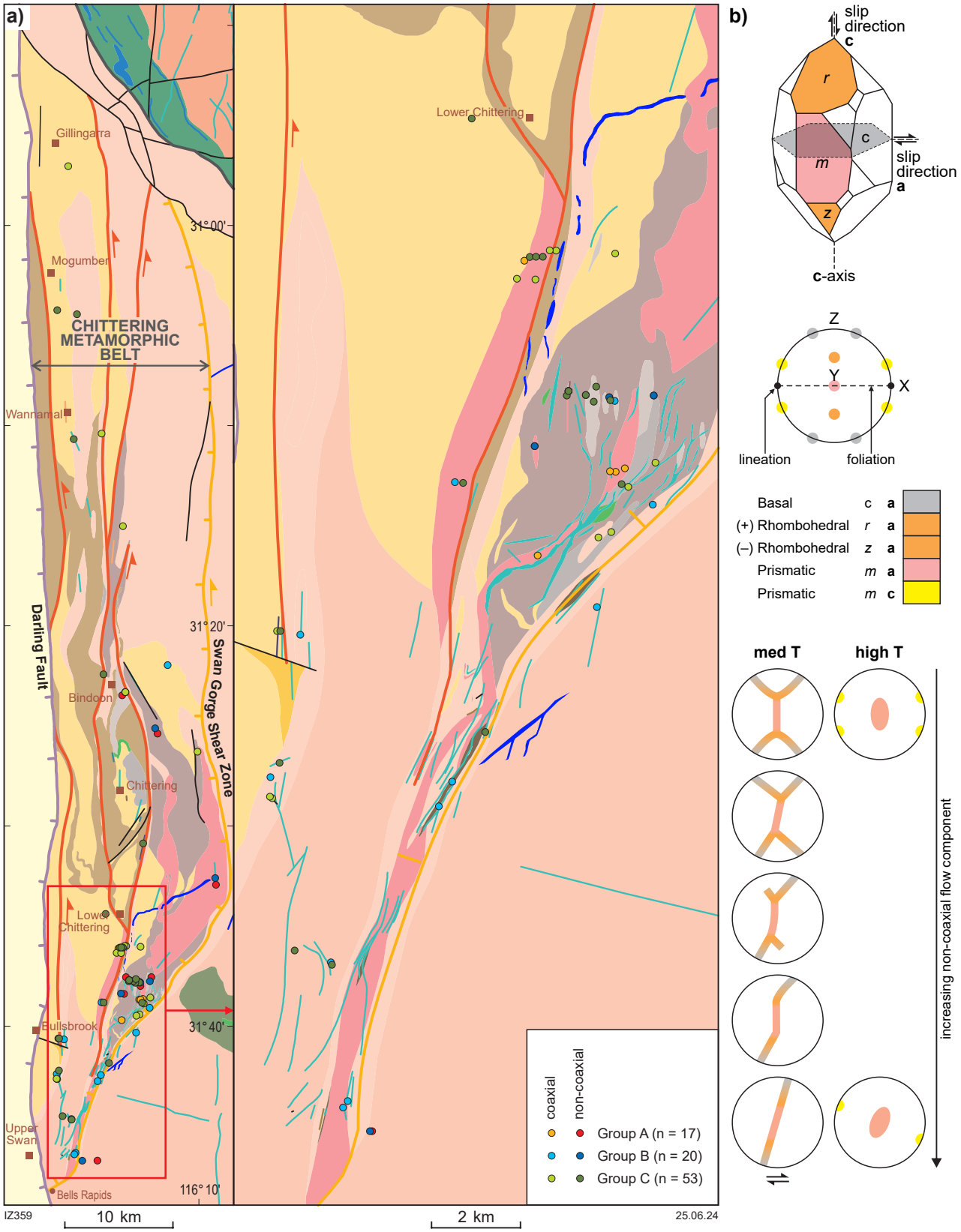

Figure 15. Quartz CPO data: a) geological map of the CMB showing the spatial distribution of samples selected for quartz CPO analysis (map's legend as per figure 5); b) essential information that allows the reader to interpret quartz CPO data presented here. Modified after Hunter et al., 2018.

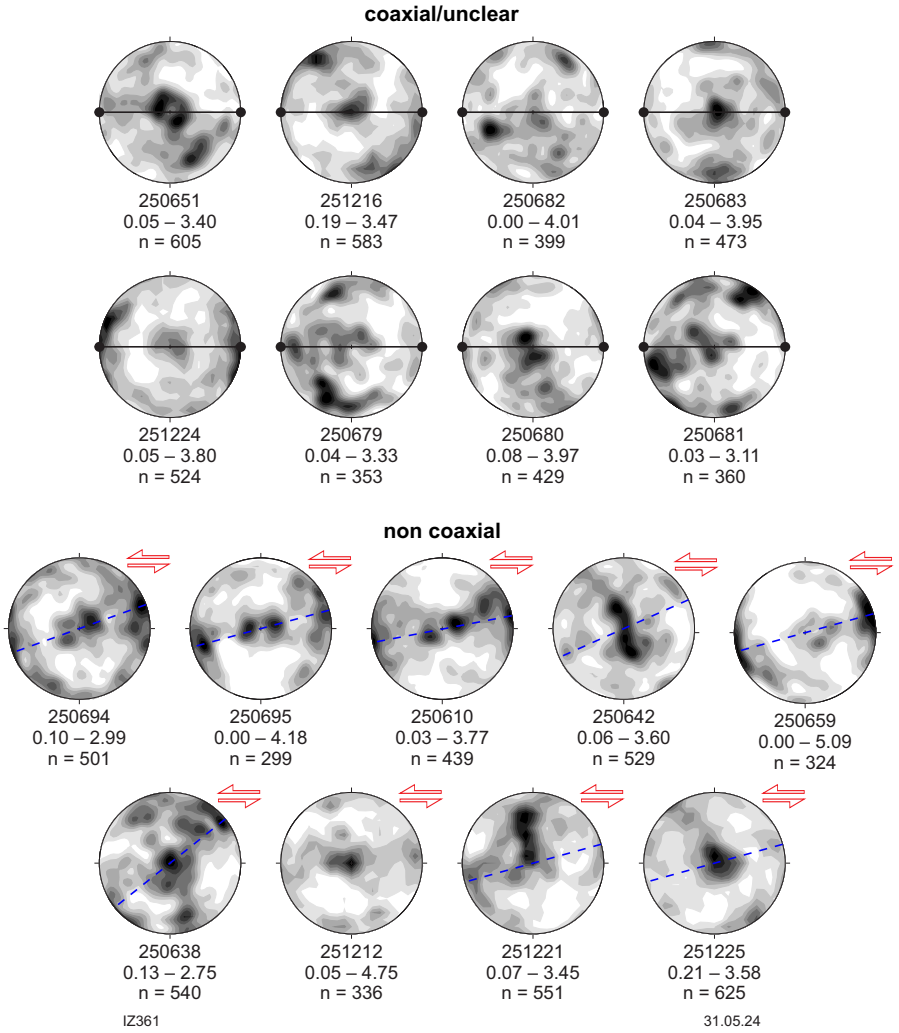

Figure 16. Samples showing high-temperature quartz CPO fabrics (group A), with maxima near the x-axis equal-area projection plots (lower hemisphere, 1% of search area). Shear plane and sense of shear are indicated for samples showing fabric with clear external symmetry. The labels show (from top to bottom): sample name, number of measurements and contour interval (multiple uniform distribution).

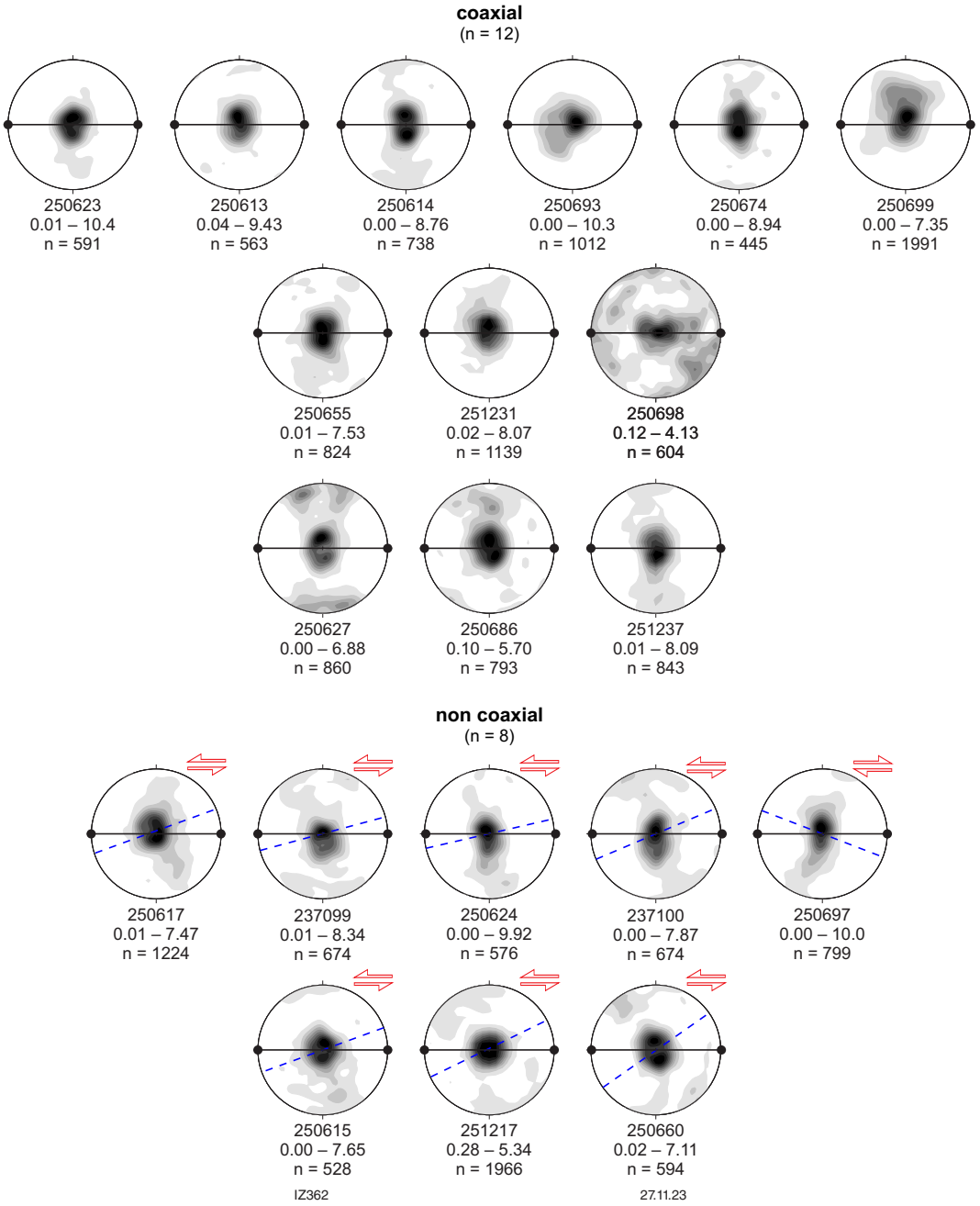

Figure 17. Samples showing a prominent maximum near the y-axis (group B) equal-area projection plots (lower hemisphere, 1% of search area). Shear plane and sense of shear are indicated for samples showing fabric with clear external symmetry. The labels show (from top to bottom): sample name, number of measurements and contour interval (multiple uniform distribution).

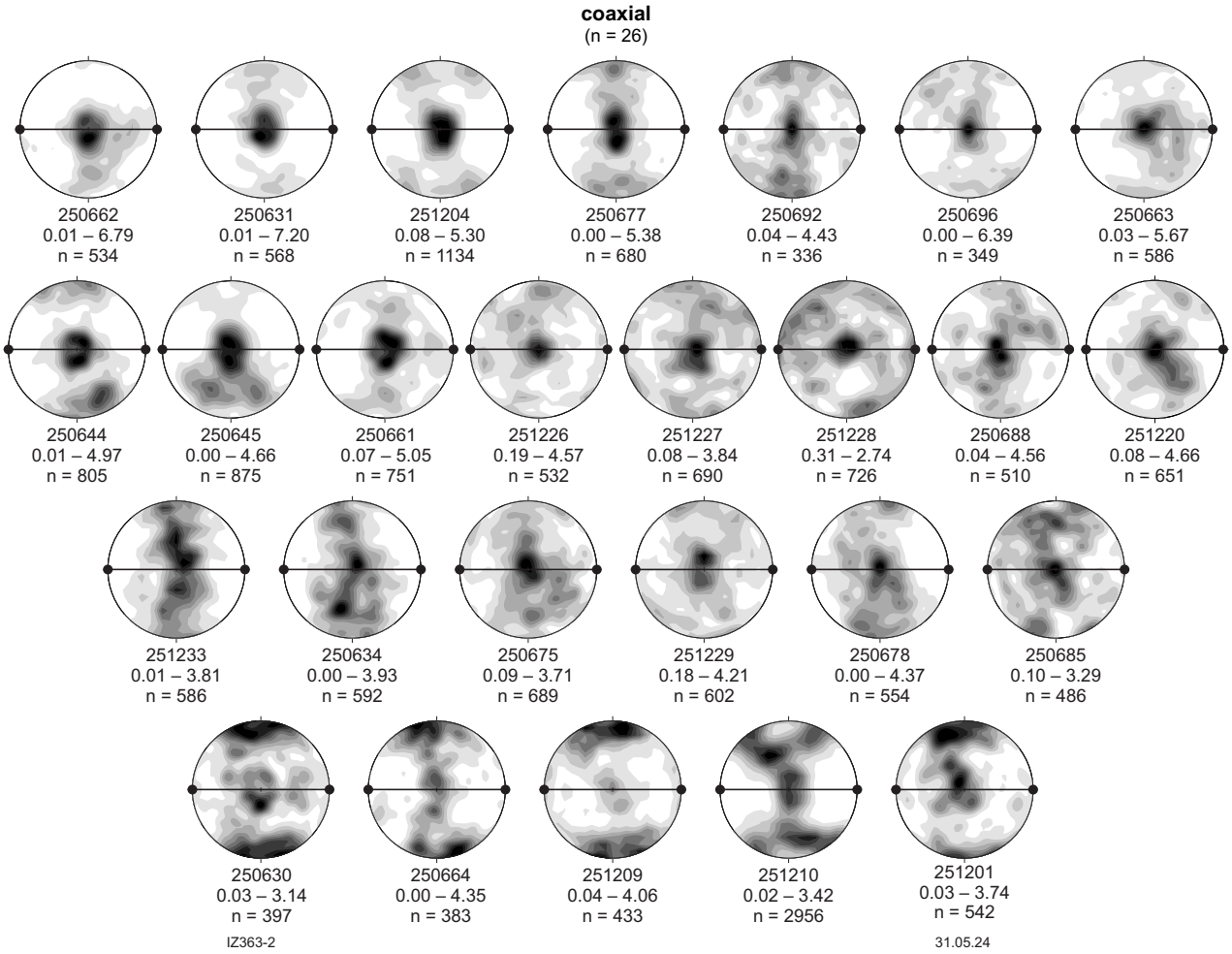

Figure 18. Samples showing a transition from maximum near the y-axis to girdle fabric and near-z maxima (group C) equal-area projection plots (lower hemisphere, 1% of search area). Shear plane and sense of shear are indicated for samples showing fabric with clear external symmetry. The labels show (from top to bottom): sample name, number of measurements and contour interval (multiple uniform distribution).

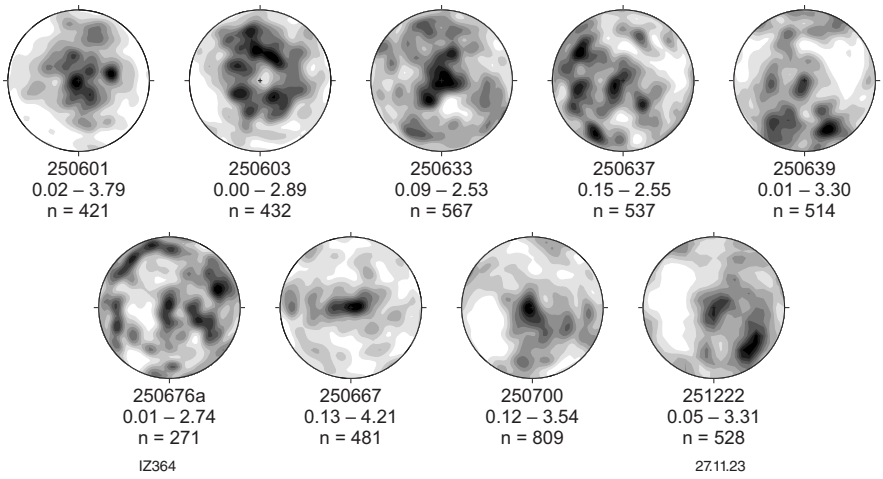

Figure 19. Equal-area projection plots (lower hemisphere, 1% of search area) from samples with maxima scattered throughout the projection plot.

Discussion and conclusions

This contribution brings together the results of a project of structural mapping along the Chittering Metamorphic Belt, a high-strain and poly-deformed portion of the Archean crust along the western margin of the Yilgarn Craton. While the area was first described and accurately mapped at 1:250 000 map scale by GSWA (Wilde and Low, 1975); since then, the CMB has not been the target of systematic geological investigations, in spite of favourable outcrop conditions and easy access. In particular, both geochronology and geochemistry characteristics of the metamorphic rock sequence that typifies the CMB are completely unknown. Therefore, the only time markers that we can use to constrain the age of the various generation of fabrics recognized within the CMB are represented by i) the 2648–2626 Ma magmatic crystallization age of the Darling Range Batholith (Nemchin and Pidgeon, 1997); and (ii) by the c. 2615 Ma magmatic crystallization age of the Yandinilling dyke swarm (Stark et al, 2018) and the c. 1200 Ma magmatic crystallization age of the north-striking gabbro–dolerite dykes (Pidgeon and Cook, 2003), widely exposed throughout the belt. Likewise, although some portions of the main highstrain zones described here had been already mentioned in previous work (Wilde and Low, 1975), and have been studied in more detail, but only at a few locations (Bretan, 1985), a systematic study of the structural evolution of the CMB was completely lacking, and represents the main goal of this contribution.

At least a dozen layered and non-layered rock types form a c. 15 km wide package in the CMB, but all can be categorized into three broad groups:

1. layered and non-layered, quartz-rich (up to ~80 modal percent), feldspar-poor to feldsparabsent, micaceous schists, with variable amounts of biotite and muscovite, and sporadic kyanite and/or sillimanite that is locally, partially to completely replaced by retrograde biotite and muscovite in intensely deformed domains (Fig. 12d). Migmatitic structures are variably developed/preserved. The bulk composition of these rocks implies a compositionally mature sedimentary protolith, although a weathered felsic igneous rock protolith cannot be completely ruled out.
2. layered migmatitic gneisses having two-mica to amphibole–biotite–titanite, tonalitic to granitic mineral assemblages. Essential plagioclase locally preserves relict igneous oscillatory zoning, suggesting felsic intrusive protoliths for these rocks.
3. rocks of bulk tonalo-granitic composition, with no visible migmatitic structures or layering. This group includes the hornblende-bearing porphyritic granite gneiss (Fig. 4a), the magnetite-bearing microgranitic gneiss (Fig. 4c), and the two-mica, equigranular granitic gneiss (Fig. 4e).

Layering in rock groups (i) and (ii) appears to result mainly from migmatization (though some layering in metasedimentary rocks might be transposed bedding); and the CMB therefore, apparently, comprises sedimentary and felsic igneous intrusive (and/or volcanic?) rocks that have been variably metamorphosed and deformed over an extended period.

The CMB therefore exposes a ~15 km thick sequence of seemingly metasedimentary and metaigneous felsic rocks – groups (i) and (ii) – which was sheared under migmatitic conditions. Remnants of mesostructures and microstructures that witnessed this high-grade tectonometamorphic event are variably preserved throughout the belt. They range from perfectly preserved migmatitic mesostructures and microstructures (Figs 8a, 13) in the low-strain domains with respect to the Proterozoic shear zones, to completely transposed migmatitic layering, in the high-strain domains. The lithological association described here is hardly comparable with the typical, mafic-dominated lithological associations of Archean greenstone belts (Hamilton, 1998).

A speculative geological history for the CMB based on existing data is illustrated in Figure 20. Protoliths apparently comprised a broadly horizontal package of siliciclastic sedimentary and felsic igneous rocks, possibly up to 15 km thick, although high strain now affecting the entire CMB and paucity of geochronology data generally preclude determination of unambiguous stratigraphic relationships between different rock units. Siliciclastic sedimentary rocks may have been deposited uncomformably on felsic igneous rocks (Fig. 20a, left), or have been intruded by them (Fig. 20a, centre), or the igneous rocks might be both older and younger than the sedimentary rocks (Fig. 20a, left).

The igneous–sedimentary association subsequently underwent shearing and migmatization at high temperatures (Fig. 20b), probably at mid- to lower crustal levels, although the actual pressure and temperature (*P–T*) conditions and tectonic setting for this high metamorphic grade event are currently unknown. Group (iii) granitic rocks were emplaced into the crust after migmatization (Fig. 20c), and the entire region was then tilted to rotate migmatite fabrics to a subvertical orientation (Fig. 20d), at some as yet indeterminate time prior to emplacement of the late-Archean Darling Range Batholith (Fig. 20e) and slightly younger, northeast-striking Yandinilling gabbro–dolerite dyke swarm (Fig. 20f), both of which appear to have been only locally deformed during later shearing events.

North-striking gabbro–dolerite dykes of the Marnda Moorn large igneous province were emplaced at c. 1200 Ma (Fig. 20g), prior to initiation of the Swan Gorge Shear Zone and Lady Springs Shear Zone in the Late Proterozoic (Fig. 20h) and their subsequent reactivation in the Phanerozoic when the Darling Fault formed in response to Gondwana breakup (Fig. 20i; Song and Cawood, 2000).

Quartz c-axis CPO data allows for tracing this long-lived tectonomagmatic evolution, and can be broadly separated into two groups: (i) group A samples, in which fabric developed at near-solidus temperature, witness the development of Archean migmatitic fabrics, and are preferentially preserved in the low-strain domains with respect to the Proterozoic shear zones; (ii) groups B and C samples reflect the retrograde evolution of the Proterozoic shear zones (SGSZ and LSSZ), from amphibolite- to greenschist-facies conditions, likely reflecting the exhumation of the CMB.

This study confirms that the high-strain CMB preserves a record of tectonomagmatic and metamorphic events spanning more than two billion years of Earth's history, and that this relatively narrow part of the western margin of the Yilgarn Craton experienced episodic shearing at locations and in orientations that were strongly controlled by early formed (inherited) fabrics. Future studies should attempt to better constrain the geochronological, geochemical and metamorphic evolution of the CMB and other parts of the western margin of the Yilgarn Craton, and determine its relationship to the evolution of the whole Yilgarn Craton.

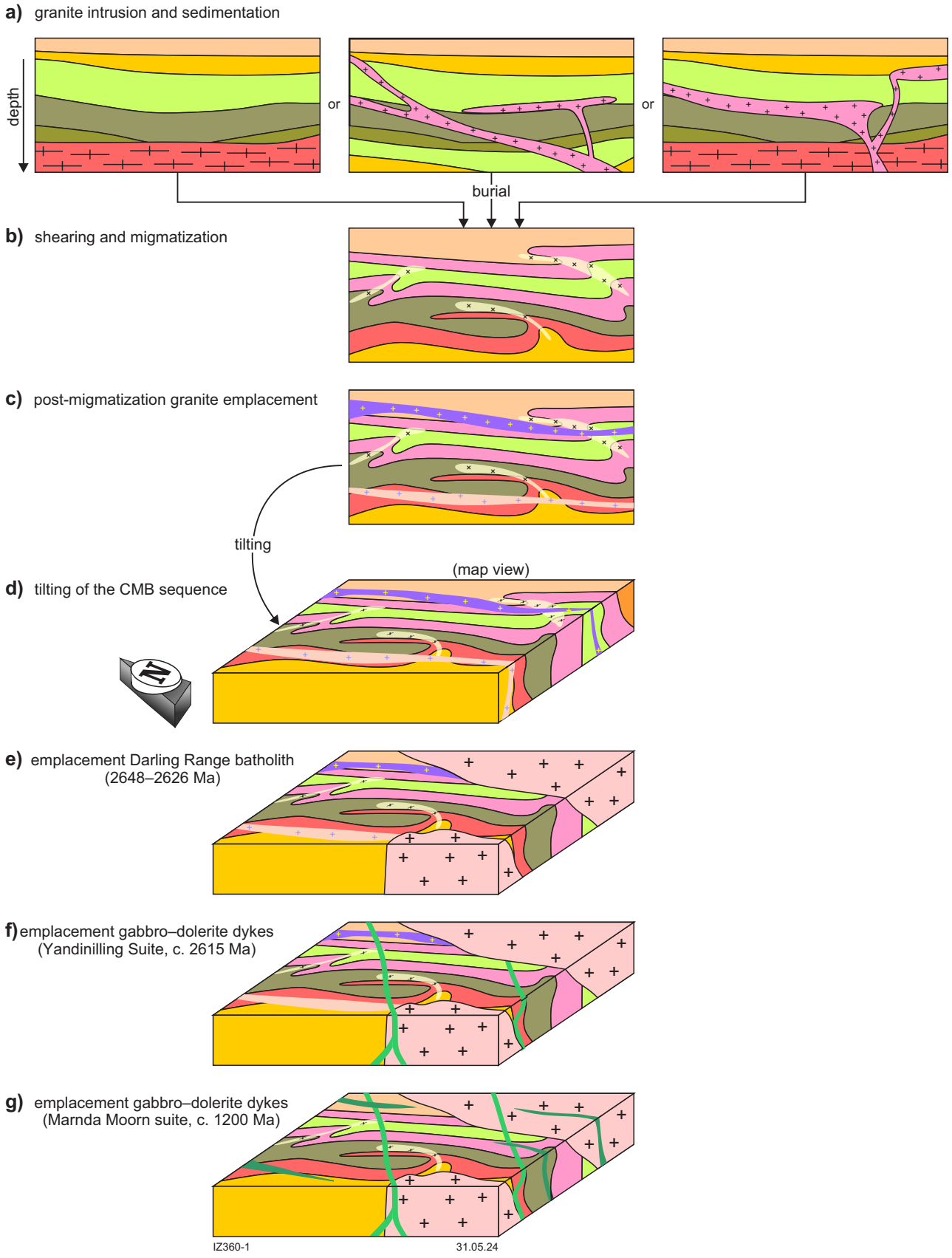

Figure 20. Cartoon illustrating the possible sequence of tectonomagmatic and metamorphic events that led to the assembly and present-day configuration of the CMB: a) the juxtaposition of metasedimentary and meta-igneous rocks could have resulted from deposition above a granitic basement (left), granite intrusion into a sedimentary sequence (centre), or a combination of both (right); b) the sequence experienced migmatization after burial, followed by granite emplacement (c), and tilting of the whole sequence (d); e) emplacement of the Darling Range Batholith along the southern portion of the CMB; f) emplacement of the Yandinilling gabbro–dolerite dyke swarm; g) emplacement of the gabbro–dolerite dykes of the Marnda Moorn suite.

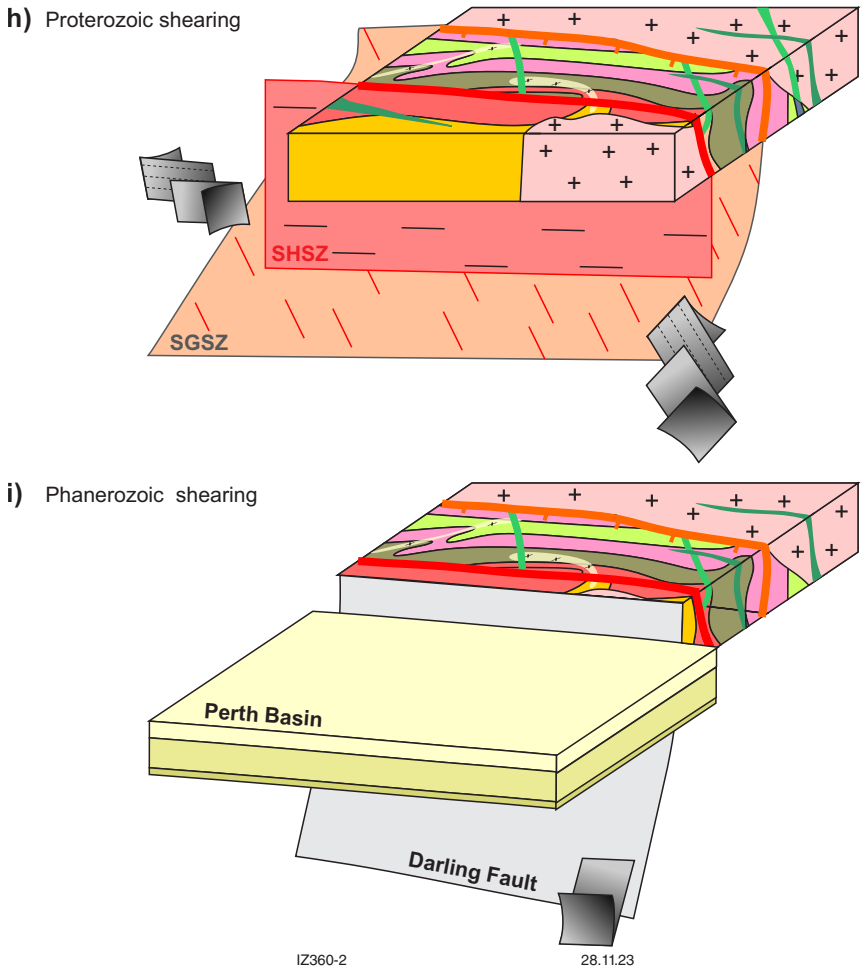

Figure 20. (continued) h) Proterozoic shearing along the Swan Gorge Shear Zone (SGSZ) and the Lady Springs Shear Zone (LSSZ); i) Phanerozoic shearing along the Darling Fault and development of the Perth Basin.

References

Blight, DF, Compston, W and Wilde, SA 1981, The Logue Brook Granite, *in* Annual report for the year 1980: Geological Survey of Western Australia, Perth, Western Australia, p. 72–80.

Bouchez, JL, Lister, GS and Nicolas, A 1983, Fabric asymmetry and shear sense in movement zones: Geologische Rundschau, v. 72, no. 2, p. 401–419, doi:10.1007/BF01822075, <http://link.springer.com/10.1007/BF01822075>.

Bretan, PG 1985, Deformation processes within mylonite zones associated with some fundamental faults: University of London.

Dentith, MC, Bruner, I, Long, A, Middleton, MF and Scott, J 1993, Structure of the Eastern Margin of the Perth Basin, Western Australia: Exploration Geophysics, v. 24, no. 3-4, p. 455–461, doi:10.1071/EG993455.

Eaton, DW and Claire Perry, HK 2013, Ephemeral isopycnicity of cratonic mantle keels: Nature Geoscience, v. 6, no. 11, p. 967–970, doi:10.1038/NGEO1950.

Fitzsimons, ICW 2003, Proterozoic basement provinces of southern and southwestern Australia, and their correlation with Antarctica: Geological Society, London, Special Publications, v. 206, p. 93–130.

Fossen, H 2016, Structural geology (2nd edition): Cambridge University Press, Cambridge, United Kingdom, 524p.

Gee, RD, Baxter, JL, Wilde, SA and Williams, IR 1981, Crustal development in the Archean Yilgarn Block, Western Australia, *in* Archaean Geology: Second International Symposium, Perth 1980 *edited by* JE Glover and DI Groves: Geological Society of Australia, Special Publication 7, p. 43–56.

Goscombe, B and Trouw, R 1999, The geometry of folded tectonic shear sense indicators: Journal of Structural Geology, v. 21, no. 1, p. 123–127, doi:10.1016/S0191-8141(98)00092-3, <http://linkinghub.elsevier.com/retrieve/pii/S0191814198000923>.

Gower, RJW and Simpson, C 1992, Phase boundary mobility in naturally deformed, high-grade quartzofeldspathic rocks: evidence for diffusional creep: Journal of Structural Geology, v. 14, no. 3, p. 301–313, doi:10.1016/0191-8141(92)90088-E.

Hamilton, WB 1998, Archean magmatism and deformation were not products of plate tectonics: Precambrian Research v.91, no. 1-2, p. 143-179.

Harris, LB 1994, Neoproterozoic sinistral displacement along the Darling Mobile Belt, Western Australia, during Gondwanaland assembly: Journal of the Geological Society, v. 151, no. 6, p. 901–904, doi:10.1144/gsjgs.151.6.0901.

Hoggard, MJ, Czarnota, K, Richards, FD, Huston, DL, Jaques, AL and Ghelichkhan, S 2020, Global distribution of sediment-hosted metals controlled by craton edge stability: Nature Geoscience, v. 13, no. 7, p. 504–510, doi:10.1038/s41561-020-0593-2.

Hunter, N, Weinberg, RF, Wilson, C and Law, RD 2018, A new technique for quantifying symmetry and opening angles in quartz c-axis pole figures: implications for interpreting the kinematic and thermal properties of rocks: Journal of Structural Geology, v. 112, p. 1–6, https://doi.org/10.1016/j.jsg.2018.04.006.

Hunter, NJ, Weinberg, RF, Wilson, C, Luzin, V and Misra, S 2019, Quartz deformation across interlayered monomineralic and polymineralic rocks: a comparative analysis: Journal of Structural Geology, v. 119, p. 118–134, doi:10.1016/j.jsg.2018.12.005.

Johnson, SP 2013, The birth of supercontinents and the Proterozoic assembly of Western Australia: Geological Survey of Western Australia, Perth, Western Australia, 78p.

Kruhl, JH 1996, Prism- and basal-plane parallel subgrain boundaries in quartz: A microstructural geothermobarometer: Journal of Metamorphic Geology, v. 14, no. 5, p. 581–589.

Law, RD 2014, Deformation thermometry based on quartz *c*-axis fabrics and recrystallization microstructures: A review: Journal of Structural Geology, v. 66, p. 129–161, doi:10.1016/j.jsg.2014.05.023.

Lister, G and Hobbs, BE 1980, The simulation of fabric development during plastic deformation and its application to quartzite: the influence of deformation history: Journal of Structural Geology, v. 2, no. 3, p. 355–370, doi:10.1016/0191-8141(80)90023-1.

Mainprice, D, Bouchez, JL, Blumenfeld, P and Tubià, JMJ 1986, Dominant c slip in naturally deformed quartz: Implications for dramatic plastic softening at high temperature: Geology, v. 14, no. 10, p. 819–822, doi:10.1130/0091-7613(1986)14<819:DCSIND>2.0.CO;2.

Mancktelow, NS and Pennacchioni, G 2005, The control of precursor brittle fracture and fluid–rock interaction on the development of single and paired ductile shear zones: Journal of Structural Geology, v. 27, no. 4, p. 645–661, https://doi.org/10.1016/j.jsg.2004.12.001.

Middleton, MF, Long, A, Wilde, SA, Dentith, M and Evans, BA 1993, A Preliminary Interpretation of Deep Seismic Reflection and other Geophysical Data from the Darling Fault Zone, Western Australia: Exploration Geophysics, v. 24, no. 3-4, p. 711–717, doi:10.1071/EG993711.

Nemchin, AA and Pidgeon, RT 1997, Evolution of the Darling Range Batholith, Yilgarn Craton, Western Australia: A SHRIMP zircon study: Journal of Petrology, v. 38, p. 625–649.

Olierook, HKH, Timms, NE, Wellmann, JF, Corbel, S and Wilkes, PG 2015, 3D structural and stratigraphic model of the Perth Basin, Western Australia: Implications for sub-basin evolution: Australian Journal of Earth Sciences, v. 62, no. 4, p. 447–467, doi:10.1080/08120099.2015.1054882.

Passchier, CW and Trouw, RAJ 2005, Microtectonics (2nd edition): Springer, Berlin, 366p.

Pearson, DG and Wittig N. 2008, Formation of Archaean continental lithosphere and its diamonds: the root of the problem: Journal of the Geological Society, v. 165, p. 895–914, doi:10.1144/0016-76492008-003.

Pidgeon, RT and Cook, TJF 2003, 1214 ± 5 Ma dyke from the Darling Range, southwestern Yilgarn Craton, Western Australia: Australian Journal of Earth Sciences, v. 50, p. 769–777.

Quentin de Gromard, R, Ivanic, TJ and Zibra, I 2021, Pre-Mesozoic interpreted bedrock geology of the southwest Yilgarn, 2021, *in* Accelerated Geoscience Program extended abstracts *compiled by* Geological Survey of Western Australia: Geological Survey of Western Australia, Record 2021/4, p. 122–144.

Rosenberg, CL and Stünitz, H 2003, Deformation and recrystallization of plagioclase along a temperature gradient: an example from the Bergell tonalite: Journal of Structural Geology, v. 25, no. 3, p. 389–408.

Schmid, SM and Casey, M 1986, Complete fabric analysis of some commonly observed quartz caxis patterns: Mineral and Rock Deformation: Laboratory Studies, v. 36, p. 263–286.

Simpson, C 1985, Deformation of granitic rocks across the brittle-ductile transition: Journal of Structural Geology, v. 7, no. 5, p. 503–511, doi:10.1016/0191-8141(85)90023-9.

Smithies, RH, Ivanic, TJ, Lowrey, JR, Morris, PA, Barnes, SJ, Wyche, S and Lu, Y-J 2018, Two distinct origins for Archean greenstone belts: Earth and Planetary Science Letters, v. 487, p. 106–116.

Song, T and Cawood, PA 2000, Structural styles in the Perth Basin associated with the Mesozoic break-up of Greater India and Australia: Tectonophysics, v. 317, no. 1–2, p. 55–72, doi:10.1016/S0040-1951(99)00273-5.

Stark, JC, Wilde, SA, Söderlund, U, Li, Z-X, Rasmussen, B and Zi, J-W 2018, First evidence of Archean mafic dykes at 2.62 Ga in the Yilgarn Craton, Western Australia: Links to cratonisation and the Zimbabwe Craton: Precambrian Research, v. 317, p. 1–13.

Stipp, M, Stünitz, H, Heilbronner, R and Schmid, SM 2002, The eastern Tonale fault zone: A 'natural laboratory' for crystal plastic deformation of quartz over a temperature range from 250 to 700 °C: Journal of Structural Geology, v. 24, p. 1861–1884.

Thomas, CM 2018, Regional seismic interpretation and structure of the southern Perth Basin: Geological Survey of Western Australia, Report 184, 52p.

Tullis, J and Yund, RA 1987, Transition from cataclastic flow to dislocation creep of feldspar: Mechanisms and microstructures: Geology, v. 15, no. 7, p. 606–609, doi:10.1130/0091-7613(1987)15%3C606:TFCFTD%3E2.0.CO;2.

Tullis, J and Yund, RA 1991, Diffusion creep in feldspar aggregates: experimental evidence: Journal of Structural Geology, v. 13, no. 9, p. 987–1000, doi:10.1016/0191-8141(91)90051-J.

Vernon, RH 2004, A Practical Guide to Rock Microstructure: Cambridge University Press, Cambridge, UK, 594p.

Wilde, SA 1999, Evolution of the Western Margin of Australia during the Rodinian and Gondwanan Supercontinent Cycles: Gondwana Research, v. 2, p. 481–499.

Wilde, SA 2001, Jimperding and Chittering Metamorphic Belts, southwestern Yilgarn Craton, Western Australia –– a field guide: Geological Survey of Western Australia, Record 2001/12, 24p.

Wilde, SA and Low, GH 1975, Explanatory notes on the Perth 1:250 000 geological sheet, Western Australia: Geological Survey of Western Australia, Record 1975/6, 67p.

Wilde, SA, Middleton, MF and Evans, BJ 1996, Terrane accretion in the southwestern Yilgarn Craton: Evidence from a deep seismic crustal profile: Precambrian Research, v. 78, p. 179–196.

Wingate, MTD 2017, Mafic dyke swarms and large igneous provinces in Western Australia get a digital makeover, *in* GSWA 2017 extended abstracts: promoting the prospectivity of Western Australia: Geological Survey of Western Australia, Record 2017/2, p. 4–8.

Zibra, I and Peternell, M 2023, Structural evolution and quartz c-axis crystallographic preferred orientation of major Yilgarn Craton shear zones: Geological Survey of Western Australia, Perth, Western Australia, Report, 55p.

RECORD 2024/3

THE CHITTERING METAMORPHIC BELT, YILGARN CRATON: STRUCTURAL SETTING, MICROSTRUCTURES AND QUARTZ CRYSTALLOGRAPHIC PREFERRED ORIENTATION

I Zibra and M Peternell

Access GSWA products

All products
All GSWA products are free to download as PDFs from the DEMIRS eBookshop <www.demirs.wa.gov.au/ebookshop>.
View other geoscience information on our website <www.demirs.wa.gov.au/gswa>.

Hard copies
Limited products are available to purchase as hard copies from the First Floor Counter at Mineral House or via the DEMIRS eBookshop <www.demirs.wa.gov.au/ebookshop>.

Fieldnotes
Fieldnotes is a free digital-only quarterly newsletter which provides regular updates to the State's exploration industry and geoscientists about GSWA's latest programs, products and services.
Access by subscribing to the GSWA eNewsletter <www.demirs.wa.gov.au/gswaenewsletter> or downloading the free PDF from the DEMIRS eBookshop <www.demirs.wa.gov.au/ebookshop>.

GSWA eNewsletter
The GSWA eNewsletter is an online newsletter that contains information on workshops, field trips, training and other events.
To keep informed, please subscribe <www.demirs.wa.gov.au/gswaenewsletter>.

Further details of geoscience products are available from:

First Floor Counter
Department of Energy, Mines, Industry Regulation and Safety
100 Plain Street
EAST PERTH WESTERN AUSTRALIA 6004
Phone: +61 8 9222 3459 Email: publications@dmirs.wa.gov.au
www.demirs.wa.gov.au/GSWApublications